Brain Topography (2026) 39:20
https://doi.org/10.1007/s10548-025-01170-7

ORIGINAL PAPER

Exploring Dynamic Alpha Band Connectivity in Parkinson's Disease: A Novel Approach to Postural Control Assessment Using the BioVRSea Paradigm

Federica Pescaglia[1] · Lorena Guerrini[1,2] · Carmine Gelormini[1] · Romain Aubonnet[3] · Gylfi Örn Thormar[4] · Giorgio Di Lorenzo[3,5] · Halldór Jónsson Jr.[1] · Mahmoud Hassan[1,6] · Hannes Petersen[7,8] · Vincenzo Minutolo[2] · Paolo Gargiulo[1,9]

Received: 26 May 2025 / Accepted: 12 December 2025 / Published online: 2 February 2026

Abstract

Parkinson's Disease (PD) is a neurological disorder characterized by impaired postural control (PC) and balance issues. To date, few studies have explored the relationship between brain activity and responses during specific tasks designed to challenge balance in individuals with PD. Our exploratory research employs an innovative paradigm to assess PC by integrating virtual reality (VR) and electroencephalography (EEG). In the study, 20 individuals diagnosed with PD who self-reported postural instability participated in the BioVRSea paradigm. This paradigm tested their PC using visuomotor stimuli and collected EEG signals to assess brain responses throughout the experiment. The results of the Parkinson's group were compared with those of 22 age-matched healthy controls (CTR). From the functional connectivity between brain regions, we extracted brain network states (BNSs) using the k-means++ clustering algorithm. These BNSs capture the dynamic organization of brain activity and were compared with canonical resting-state networks (RSNs) to investigate neural alterations in individuals with PD. Six distinct BNSs were identified, with the dorsal attention network (DAN) dominant in five states. A significant reduction in the coverage of BNS2 was observed in PD patients during both the PRE (adjusted p-value = 0.019) and MOV (adjusted p-value = 0.036) phases compared to CTR. This reduced BNS2 coverage suggests impaired visuomotor integration in PD patients during PC tasks. DAN dominance highlights its crucial role in maintaining attentional control during the task. The findings of this study highlight the potential of using brain dynamics as a biomarker of neural dysfunction in PD, especially during specific PC tasks. Altered BNSs, particularly in networks associated with attention and sensorimotor integration, reveal key neural deficits related to PD.

Keywords Postural Control · Electroencephalography · Parkinson's Disease · Brain Network States

Federica Pescaglia and Lorena Guerrini have contributed equally to this work and shared the first authorship.

Communicated by Micah Murray.

✉ Paolo Gargiulo
paolo@ru.is

[1] Institute of Biomedical and Neural Engineering, Reykjavik University, Reykjavik, Iceland

[2] Department of Mathematics, Physics and Engineering Applications, University of Campania L. Vanvitelli, Caserta, Italy

[3] Laboratory of Psychophysiology and Cognitive Neuroscience, Department of Systems Medicine, University of Rome Tor Vergata, Rome, Italy

[4] Department of Neurology, Landspitali University Hospital, Reykjavik, Iceland

[5] IRCCS Fondazione Santa Lucia, Rome, Italy

[6] MINDIG, Rennes, France

[7] Department of Anatomy, School of Health Sciences, Biochemistry, University of Iceland, Reykjavik, Iceland

[8] Department of ORL Head and Neck Surgery, Akureyri Hospital, Akureyri, Iceland

[9] Department of Science, Landspitali University Hospital, Reykjavik, Iceland

Abbreviations

ALFF	Amplitude of Low-Frequency Fluctuations
ASR	Artifact Subspace Reconstruction
AUD	Auditory Network
BL	Baseline Phase
BNS	Brain Network State
CTR	Healthy Controls
DAN	Dorsal Attention Network
DMN	Default Mode Network
EEG	Electroencephalogram
EMG	Electromyogram
GEV	Global Explained Variance
GFP	Global Field Power
GMD	Global Map Dissimilarity
ICA	Independent Component Analysis
LMM	Linear Mixed Model
MOT	Motor Network
MOV	Movement Stimulus Phase
MS	Motion Sickness
NEURO	Neurological/Muscle Strain Index
PC	Postural Control
PD	Parkinson's Disease
PDnonVH	PD Patients without Visual Hallucinations
PHY	Physiological/Vegetative Index
PLV	Phase-Locking Value
POST	Post-Motor Stimulus Phase
PRE	Pre-Motor Stimulus Phase
ROI	Region Of Interest
RSN	Resting-State Network
SAN	Salience Network
TP	Transition Probabilities
V1	Primary Visual Cortex
VIS	Visual Network
VR	Virtual Reality
wMNE	weighted Minimum Norm Estimate

Introduction

Parkinson's disease (PD) is a widespread neurodegenerative condition characterized by tremors, stiffness, slowed movements, and balance problems (Tolosa et al. 2006). In addition to these motor symptoms, individuals with PD often experience non-motor symptoms such as cognitive decline, mood disorders, difficulty with speech, and swallowing. Symptoms usually progress slowly, affecting the ability to perform daily activities and significantly affecting the quality of life. As the brain struggles to respond accurately to external stimuli, motor tasks in people affected by PD become increasingly challenging, leading to a greater impact of neurodegeneration (Shumway-Cook and Woollacott 2007; Woollacott and Shumway-Cook 2002). The diagnosis of PD is a significant clinical challenge due to the overlap of motor and non-motor symptoms with other pronounced neurological deficits (Kilzheimer et al. 2019). Early signs can often be mistaken for typical age-related changes, complicating the diagnostic process. Since there are no definitive biomarkers for PD, the diagnosis is primarily based on clinical evaluations along with a range of diagnostic tools. These include gait analysis to assess motor function, brain imaging techniques like MRI or PET scans to detect structural or functional changes in the brain, and electroencephalography (EEG) to monitor electrical activity. These approaches are essential in helping clinicians distinguish PD from other conditions with similar symptoms, although an accurate diagnosis can still be challenging. Studies on quantitative gait analysis have demonstrated that measures such as stride length, gait speed, and variability in step timing can effectively differentiate PD from other movement disorders, as shown by (Hausdorff 2009). The technique is especially valuable for monitoring the progression of PD and evaluating the effectiveness of treatments, such as levodopa (Del Din et al. 2016). On the other hand, brain imaging techniques offer critical insight into structural and functional anomalies associated with PD. Magnetic resonance imaging (MRI) is primarily used to exclude other neurological conditions and can also highlight subtle alterations in structures such as the substantia nigra (Morris et al. 2005). However, it is limited in its ability to detect early neurodegenerative changes associated with PD. Functional imaging techniques, such as Positron Emission Tomography (PET) and Single Photon Emission Computed Tomography (SPECT), provide more specific information by visualizing the dopaminergic deficits common in PD (Brooks 2010; Benamer et al. 2000). Emerging techniques, such as near-infrared spectroscopy (NIR), are also gaining attention due to their potential to assess cortical hemodynamics and oxygenation patterns in PD. NIR offers a non-invasive means of examining brain function, with recent studies suggesting it could be a useful adjunct to other imaging modalities in diagnosing PD (Schwarz et al. 2014).

EEG has emerged as a complementary diagnostic tool for PD, showing great potential due to its unique advantages in terms of temporal resolution (Mulert 2013; Hassan and Wendling 2018; Sakkalis 2011). Compared to more expensive imaging methods like PET or MRI, EEG is not only cost-effective but also portable, making it suitable for use in various clinical environments. Additionally, it is non-invasive, requiring no exposure to radiation or contrast agents. EEG records brain activity with millisecond precision, enabling the monitoring of fast neural dynamics linked to motor control and cognition. This real-time insight is particularly valuable in PD, where the progressive degeneration of dopaminergic neurons disrupts brain-body communication.

EEG can detect these disruptions as they occur, potentially revealing alterations in neural activity patterns before symptoms like tremors or bradykinesia emerge. The ability to detect early neural changes underscores the potential of EEG in identifying preclinical or early-stage markers of PD, as shown in recent studies (Molcho et al. 2023; Aljalal et al. 2022; Zhang et al. 2022). Moreover, its ability to examine changes in brain connectivity and resting-state networks, often disrupted in PD, provides an added layer of diagnostic capability.

Furthermore, EEG is increasingly being recognized for its role in assessing PC in neurological disorders (Priplata et al. 2003; Niedermeyer and da Silva 2005). PC refers to the complex integration of sensory inputs, motor responses, and neural processes that help maintain balance and stability (Mancini and Horak 2010; Winter 1995). In PD, the progressive degeneration of dopaminergic neurons disrupts these mechanisms, leading to postural instability, which significantly increases the risk of falls and injuries (Kelly et al. 2015; Xu et al. 2014). Studies have shown that PD patients demonstrate irregular brainwave patterns during PC tasks. Recent research has linked alpha band activity in EEG to various aspects of PC, including balance maintenance and postural adjustments (Ma et al. 2022; Lanthier et al. 2020; Woo and Lee 2019). For instance, increases in alpha power are associated with improved postural stability (Balasubramaniam and Wing 2002; Doblhoff and Friedl 2018), while decreases indicate greater attention demands or instability (Del Percio et al. 2007?). Alpha coherence between brain areas has been shown to play a role in sensory processing and motor planning, both of which are important for maintaining balance (Hülsdünker et al. 2015; Dos and Santos 2013). The integration of sensory information becomes particularly challenging in PD, where patients exhibit a reduced capacity to combine input from the body and environment. EEG analyses reveal disrupted connectivity and decreased synchronization among brain regions involved in sensory integration and motor planning, such as the sensorimotor cortex and parietal areas (Araújo-Silva et al. 2022). In line with the alterations reported in alpha power and coherence during PC tasks, these dysfunctions include reduced alpha-band coherence between cortical regions, impaired sensory reweighting mechanisms, and decreased functional connectivity within sensorimotor and parietal networks. Together, these alterations disrupt the integration of sensory inputs and motor planning processes, significantly contributing to the postural instability characteristic of PD.

Most EEG investigations in PD focus on resting-state and static tasks, leaving a gap in understanding brain activity during dynamic tasks requiring continuous postural adjustments. Our study introduces a new paradigm called BioVRSea, a system designed to stimulate PC responses using a virtual reality (VR) environment and a moving platform. Previous studies have demonstrated the effectiveness of BioVRSea as a tool for evaluating PC (Stehle et al. 2022; Aubonnet et al. 2022). Moreover, this setup has proven to be a promising tool for developing predictive models for various conditions (Recenti et al. 2022, 2023), including individuals who have experienced concussions or suffer from motion sickness (Jacob et al. 2022b). A recent study using the BioVRSea paradigm has revealed significant differences in theta and alpha power spectra bands between early-stage PD patients and healthy controls, highlighting its potential to offer deeper insights into the neural mechanisms behind postural instability in PD (Jacob et al. 2023).

The BioVRSea paradigm differs from conventional PC assessment tools in that it combines VR–induced sensory conflicts with EEG recordings, allowing for the detection of neurophysiological alterations that may not yet manifest as overt motor impairments. Unlike standard laboratory tasks, BioVRSea also offers high ecological validity, as its multisensory VR environment actively engages visual, vestibular, and proprioceptive senses, more closely mimicking the complex and dynamic balance demands encountered in real-life situations. Traditional dynamic PC assessments-such as gait analysis or force-platform–based balance tests-primarily quantify behavioral or kinematic changes (e.g., stride length, sway amplitude), which are sensitive to later stages of motor dysfunction but less specific to early neural alterations. By contrast, BioVRSea allows for simultaneous monitoring of brain and postural responses during dynamic balance challenges, offering a more sensitive and integrative assessment of PC. Moreover, it provides a more specific evaluation of PD-related postural deficits, capturing subtle neural and motor adaptations, and the combination of visual onset and motor stimulation makes the paradigm uniquely suited to detect early PD alterations.

The evaluation of PC response using a dynamic approach on EEG, such as the identification of brain network states (BNSs), has recently demonstrated significant potential (Aubonnet et al. 2023). In recent years, advanced EEG techniques have been developed to analyze functional connectivity by reconstructing brain sources from scalp signals and identifying brain networks. The BNSs refer to specific patterns of connectivity in the brain that change to adapt to various demands and environments (Petersen and Sporns 2015; Cohen 2015). In PC, maintaining balance and stability requires the integration of sensory information, motor planning, and cognitive processes, all of which are influenced by the activity of distinct brain networks. Altered BNSs in PD have been identified through fMRI and EEG, showing disrupted connectivity in critical networks related to motor control, attention, and sensorimotor integration (Tessitore et al. 2014). These alterations affect regions like

the supplementary motor area and primary motor cortex during both rest and motor tasks. Additionally, the altered BNS configurations in PD impact cortical-striatal circuits involved in motor planning. These results reflect how the neurodegenerative disease affects the dynamic reconfigurations of the brain and present potential biomarkers for diagnosis and tracking progression. Established networks, including the default mode network, the auditory network, the salience network, the executive control network, and the sensorimotor cortex, have been linked to specific cognitive tasks and postural adjustments (Lv et al. 2018; Shirer et al. 2012). These networks are crucial for balance-related processes, highlighting their significance in maintaining stability and coordinating motor function (Raichle 2015; Fox and Raichle 2007). Furthermore, disruptions in BNS can lead to impaired PC, which is particularly evident in individuals with neurodegenerative conditions such as PD. By studying BNSs in relation to PC, research can identify potential biomarkers for diagnosing balance disorders and tracking disease progression.

The study introduces several innovations for the evaluation of early-stage PD, in particular during a complex PC task. A key advancement is the use of dynamic EEG analysis to identify brain networks in PD. These BNSs provide a deeper understanding of the functional organization of the brain during our experiment, offering insights into how the brain adapts to different tasks and conditions. While there is no universally defined optimal method for processing EEG data to identify brain networks, we employed the most advanced methodologies, which have shown the best performance in previous studies (Hassan et al. 2014). This approach allows for a more precise analysis of brain connectivity, enhancing our understanding of PD progression and treatment responses.

With BioVRSea, we computed functional brain connectivity activity during dynamic balance challenges, identifying the BNSs associated with attention, visuomotor integration, and sensory processing. Our study demonstrated that PD patients exhibit deficits in dorsal attention and sensorimotor networks. These neural markers were observed in early-stage PD participants without overt motor symptoms, indicating high sensitivity of the BioVRSea paradigm in detecting subtle, disease-related neural dysfunctions.

Table 1 Age and gender distribution in PD and CTR groups. No significant differences were found (t-test for age, chi-squared test for gender)

	PD (n=20)	CTR (n=22)	p-value
Age			0.182
Mean ± SD	65.4 ± 4.50	62.8 ± 4.27	
Min-Max	54–82	55–72	
Gender (%)			0.817
Female	8 (40%)	12 (54.5%)	
Male	12 (60%)	10 (45.5%)	

The nature of this work is exploratory, as we focus on investigating a specific frequency range, the alpha band. No previous study has focused on PD during a specific visuomotor task while investigating brain dynamics. By analyzing BNSs during the BioVRSea paradigm, a task that is both cognitively and motorically demanding, we aim to identify neurophysiological markers of PD. Our findings could contribute to early-stage diagnosis by detecting changes in brain connectivity and motor control mechanisms associated with PD.

Materials and Methods

Participants

Participants were recruited between 18/01/2022 and 03/10/2023. Informed consent was obtained from all participants before their inclusion in the study. The Icelandic National Bioethics Committee approved the study protocol with the consent *VSN-20–101* for the healthy cohort and extended it to include the Parkinson's cohort under amendment *VSN-20–101-V2*. The study involved 42 participants: 20 PD patients (54–82 years old, mean age=65.35) and 22 age-matched healthy control (CTR) individuals (55–72 years old, mean age=62.78). Table 1 demonstrates that neither the t-test for age nor the chi-squared test for gender revealed any significant differences, indicating homogeneity in the population characteristics between the two groups. Participants in the PD group had a diagnosis of early-stage PD, and they were under levodopa medication. All patients were tested in their ON medication state, as confirmed by the absence of visible motor symptoms during the experimental session. The mean disease duration at the time of testing was approximately 1–2 months, confirming that all patients were evaluated very early after diagnosis. The Hoehn and Yahr (H/Y) scale (Bhidayasiri et al. 2012) was used to classify disease stage, with values ranging from 1 to 3. Following clinical evaluation, 11 patients showed no signs of cognitive decline, while the remaining participants were classified as having mild cognitive impairment (MCI). None were diagnosed with Parkinson's dementia. Consistent with both the medical screening performed before participation and our direct observations during data acquisition, none of the patients exhibited visible tremor, dyskinesia, or other involuntary movements throughout the BioVRSea experiment. All participants completed the full experiment and responded to both the pre-experiment and the post-experiment questionnaire. From these responses, we did not register any cognitive issues or impairments.

BioVRSea Paradigm

The multi-biometric BioVRSea setup simulates a sea environment where the subject is positioned on a small virtual boat synchronized with a moving platform. The innovative system, shown in Fig. 1, integrates EEG with VR to induce and assess PC through various visuomotor stimulations. This environment is designed to create a sensation of imbalance, prompting the participant to engage in postural strategies to maintain equilibrium. The movement of the platform introduces a dynamic balance challenge, which becomes particularly pronounced towards the end of the experiment. Data acquisition during the experiment is systematically conducted by integrating various measurement systems, including EEG, electromyography, heart rate variability, electrodermal activity, and a force platform. These data are integrated to compare PC between individuals. In this study, we focused exclusively on the EEG data and did not include the other measurements in our comparisons.

The experimental protocol is divided into four main phases, each designed to elicit coordinated sensory, motor, and postural responses, as depicted in Fig. 1. It begins with the baseline phase (BL), during which the participant stands on a platform with their arms relaxed at their sides for two minutes after the start of the acquisition. During this phase, the VR environment displays a mountainous landscape to activate all sensors and prepare the system for the upcoming experiment. This is followed by the pre-motor stimulus phase (PRE), during which visual stimuli simulating ocean waves are presented through the VR goggles. Then, the platform begins to move, initiating the movement-stimulus phase (MOV), during which participants are asked to grasp a bar. The platform executes synchronized movements of varying amplitudes, integrating motor and visual stimuli. The experiment concludes with the post-motor stimulus phase (POST), during which the movement of the platform is suddenly stopped while the VR sea simulation continues. In this phase, participants are required to maintain their balance without holding the bar again, as only visual stimuli are presented. This phase introduces the additional challenge of residual instability from the earlier platform movements. The previously listed phases (PRE, MOV, and POST) each last 40 seconds, bringing the total experiment duration to approximately five minutes.

BioVRSea aims to measure the latency between the pre-motor phase and the post-motor phase following the induction of movement. This comprehensive approach aims to understand the physiological responses elicited by the BioVRSea simulation, providing valuable insights into complex PC tasks under conditions of sensory conflict.

Questionnaire

Before the experiment, each participant completes a questionnaire designed to gather information about their physical condition, neural status, lifestyle, and family history. Additionally, participants answer questions inspired by Golding's Motion Sickness Susceptibility Questionnaire (MSSQ) (Golding 2006) to assess past MS symptoms. Symptoms such as general discomfort, headache, increased salivation, sweating, and dizziness are used to calculate the BioVRSea Effect Index (BVSEI), which measures changes in symptoms before and after the VR simulation. This index classifies individuals into two groups: those who experience

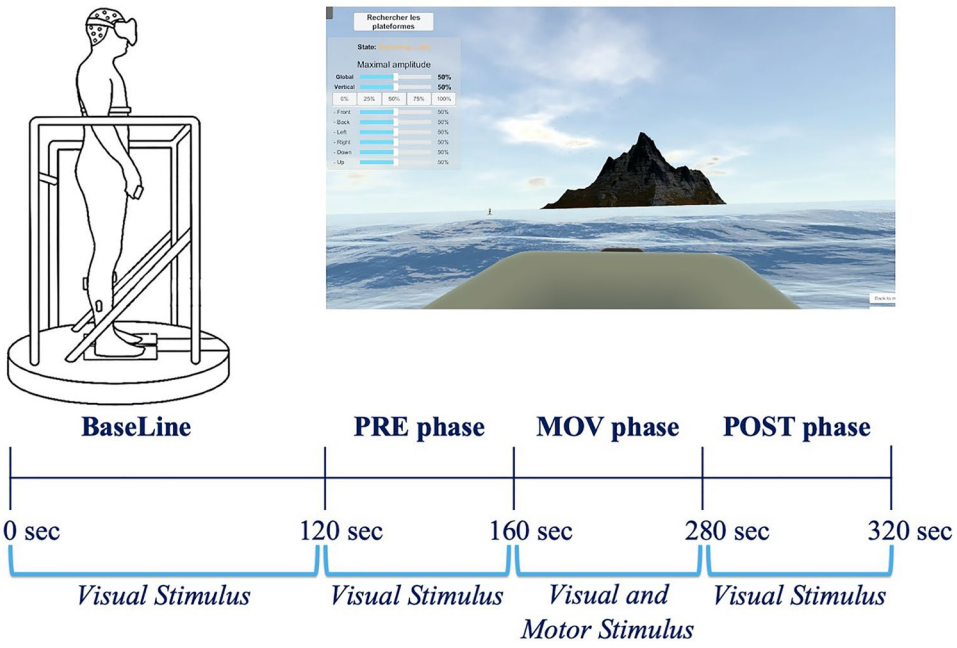

Fig. 1 BioVRSea. The different phases of the simulation are characterized by distinct types of stimulation: baseline phase (BL; 0–120 sec) with a mountainous landscape and no motor stimulation; pre-motor stimulus phase (PRE; 120–160 sec) with the visual simulation of the boat; movement-stimulus phase (MOV; 160–280 sec) with visuomotor stimulation and the platform moving at different amplitudes; post-motor stimulus phase (POST; 280–320 sec) with only visual stimulation remaining after the platform stops moving

one or more symptom changes after the simulation and those who do not experience any changes (Recenti et al. 2021). Understanding these symptom changes is particularly relevant for individuals with neurodegenerative conditions, as these diseases can impact postural stability and exacerbate symptoms during tasks requiring balance. The Lifestyle Index is calculated based on responses regarding BMI, physical activity, and consumption of nicotine, caffeine, and alcohol, all of which can influence both overall health and the management of neurodegenerative diseases. Further, two more indices are established: the Physiological/Vegetative (PHY) and Neurological/Muscle Strain (NEURO) indices (Recenti et al. 2021). Both indices are calculated based on the difference in symptoms before and after the experiment. The PHY index is based on responses regarding general discomfort, increased salivation, sweating, and nausea, while the NEURO index focuses on general discomfort, fatigue, headache, blurred vision, and dizziness. These indices are crucial for evaluating the effects of the VR simulation on the PC of the participants, especially for those with neurodegenerative diseases that can impair their ability to maintain balance and coordination.

Data acquisition

EEG data were recorded using a WaveGuard EEG cap, 64 channels (CA-201; ANT Neuro, Hengelo, Netherlands) with a sampling frequency of 4096 Hz, following the 10–10 system for electrode placement (Table 2). The EEG cap was connected to the ANT Neuro eego amplifier (EE-2XX; ANT Neuro, Hengelo, Netherlands), which interfaced with a tablet for data acquisition. The coupling between the cap and the amplifier is supported by the amplifier's design, which includes a very high input impedance (>1 GΩ) and active shielding technology, allowing reliable operation even at higher electrode–scalp impedance levels. Electrode contact was ensured using conductive gel, applied via a blunt needle syringe to maintain low impedance between the scalp and the electrodes, keeping values below 40 kΩ. This threshold is consistent with the specifications of the ANT Neuro eego amplifier used in the BioVRSea setup. According to ANT Neuro's technical documentation, high-quality EEG signals can be maintained even when impedances are relatively high (ANT Neuro 2023). In addition, the preprocessing pipeline provides robust attenuation of noise related to electrode contact variability, ensuring that data quality remains adequate for source reconstruction despite the higher impedance range.

Table 2 EEG cap. Electrode placement across different brain lobes for the WaveGuard EEG cap

Lobes	Electrode names
Frontal	FP1, FPz, FP2, AF7, AF3, AFz, AF4, AF8, F7, F5, F3, F1, Fz, F2, F4, F6, F8, FC3, FC1, FCz, FC2, FC4, C3, C1, Cz, C2, C4
Temporal Left	FT7, FC5, T7, C5, TP7, CP5
Temporal Right	FC6, FT8, C6, T8, CP6, TP8
Parietal	CP3, CP1, CPz, CP2, CP4, P7, P5, P3, P1, PZ, P2, P4, P6, P8
Occipital	PO7, PO3, POz, PO4, PO8, O1, Oz, O2

Data Pre-processing

Signal pre-processing was performed using the EEGLAB Matlab toolbox to eliminate artifacts, eye blinking, and line noise. Each signal was manually inspected to customize our pipeline. The EEG signals were down-sampled to a frequency of 1024 Hz from the original sampling rate. A dual-filter approach was applied, incorporating a high-pass filter at 1 Hz and a low-pass filter at 45 Hz to enhance signal clarity and diminish noise interference. Channels with flat signals or a correlation coefficient below 60% from neighboring channels were excluded from further analysis as noisy channels. The initial step in artifact removal utilized the Artifact Subspace Reconstruction (ASR) method (Kothe and Jung 2016). Then, independent component analysis (ICA) was performed using the probabilistic ICA for reliable data (PICARD) method (Ablin et al. 2018), known for its effectiveness in handling dynamic recordings. Non-brain components were rejected during this step. Afterward, the previously removed and flat channels were interpolated, while the mastoid electrodes (M1 and M2), along with PO5 and PO6, which measure neck activity, were excluded from the analysis. Finally, the remaining channels (excluding EOG) were interpolated back to 61, and the data were re-referenced to the average.

Data Processing: Connectivity Analysis to Dynamic Network Computation

Several preliminary steps were required before computing the dynamic brain networks, as described in Fig. 2. EEG source connectivity is a valuable method for identifying brain networks linked to specific cognitive functions, as demonstrated by Hassan et al. (Hassan et al. 2014).

The first step was the reconstruction of brain sources from the signals recorded on the scalp. In fact, estimating connectivity directly from the sensor level is limited by low spatial resolution and the effects of volume conduction. These issues can cause false correlations in connectivity measurements, as signals from different electrodes may originate from the same neural source. As a result, connectivity at the sensor level does not accurately reflect functional interactions between brain areas. To address this, we used EEG source localization techniques to reconstruct cortical activity, which involves solving the complex EEG

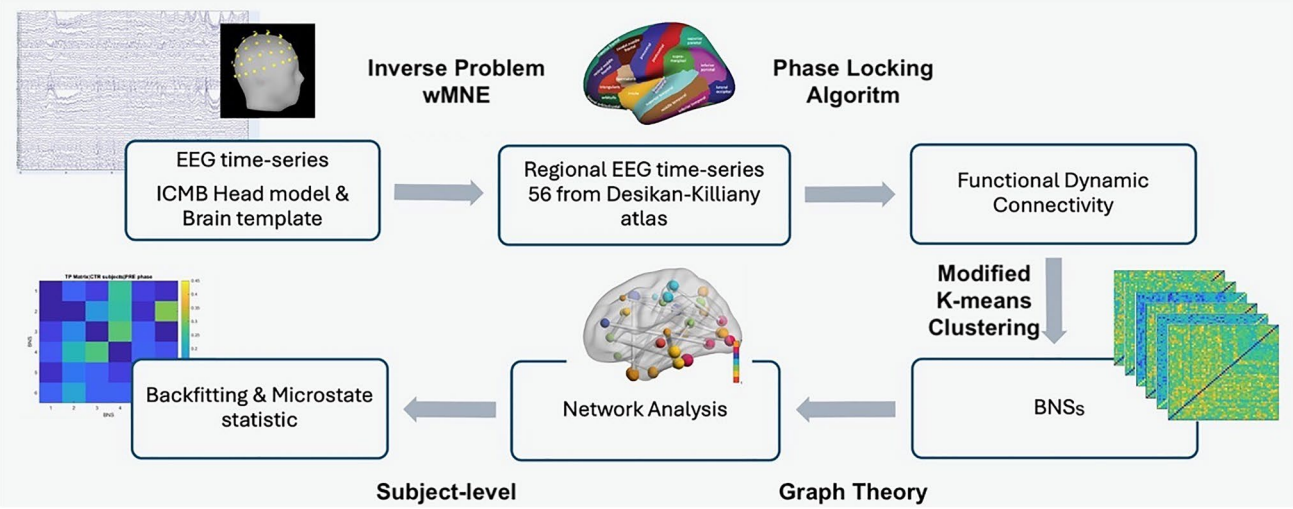

Fig. 2 Workflow description. EEGs were recorded using 64 electrodes during the BioVRSea experiment. The cortical sources were reconstructed by solving the inverse problem using the wMNE method. After source reconstruction, the signals were divided into 56 brain Regions Of Interest (ROIs) derived from the Desikan–Killiany atlas, originally composed of 68 ROIs. The reduction to 56 ROIs was performed to address the spatial resolution limitations of EEG source estimation by aggregating anatomically related regions, and to ensure methodological consistency with the network analysis by selecting ROIs according to their assignment to the seven canonical Resting-State Networks (RSNs). Functional connectivity matrices were computed between the 56 regional time series using the PLV method across five frequency bands (Delta, Theta, Alpha, Beta, Gamma). Connectivity matrices were first obtained separately for the PD and CTR groups, then concatenated before being input into the k-means++ clustering algorithm. This clustering process identified distinct Brain Network States (BNSs), followed by network analysis at the subject level to compute metrics for group comparisons

inverse problem. The neural sources for artifact-free EEG data were estimated using the following equation.

$$S = GD + N \tag{1}$$

where $S(t)$ represented the EEG signals recorded at M electrodes, G is the lead field matrix that models how sources contribute to the scalp potentials, $D(t)$ denotes the unknown brain activity at P source locations, and $N(t)$ accounts for noise and modeling errors. To solve the inverse problem, we used the *Weighted Minimum Norm Estimate (wMNE)*, given by the formula:

$$D_{wMNE} = (G^T W G + \lambda I)^{-1} G^T W S \tag{2}$$

where G is the lead field matrix, W is a depth-weighting matrix, λ is a regularization parameter, and S represents the EEG signals.

We used the ICBM MRI template with three-layer segmentation (scalp, outer skull, and inner skull) from the OpenMEEG plugin within the Brainstorm toolbox. The Boundary Element Method (BEM) was employed to model the head volume conductor, validated by prior research (Edmunds et al. 2019; Kabbara et al. 2021; Barollo et al. 2022). The initial 45 seconds of the EEG were used to construct the noise covariance matrix, while the remaining 273 seconds were allocated for source reconstruction.

The signals were then divided into 56 brain regions of interest (ROIs) derived from the Desikan-Killiany atlas (Desikan et al. 2006), which originally contains 68 ROIs, aiming for a lower number of ROIs, to address the low spatial resolution issue of EEG and the effect on the accuracy of source estimation (Guttmann-Flury et al. 2025; Farahibozorg et al. 2018; Lopes et al. 2020). Moreover, to ensure consistency with the network analysis performed in this study, those ROIs were selected based on their assignment to the seven canonical RSNs, emphasizing the functional response of brain dynamics to BioVRSea. This resulted in a final set of 56 ROIs (Appendix ROI-Node-RSN Mapping).

Functional connectivity between the EEG time series of the 56 ROIs was calculated across multiple frequency bands (Delta: 1–4 Hz, Theta: 4–8 Hz, Alpha: 8–13 Hz, Beta: 13–30 Hz, Gamma: 30–45 Hz) using the Phase-Locking Value (PLV) algorithm with a sliding window approach (50% overlap and window size of six cycles) (Lachaux et al. 2000). The combination of wMNE and PLV demonstrated optimal performance in capturing meaningful brain network dynamics in the alpha band during complex postural control tasks (Hassan et al. 2014; Aubonnet et al. 2023).

The PLV computation produced 56x56 square dynamic matrices for each band. The number N, representing the total number of computed connectivity matrices, is detailed in Appendix Phase-Locking Value (PLV) Calculation.

Table 3 Dynamic Connectivity Variables. A list of the number of matrices (N) calculated for each frequency band. The dimension (n) of each matrix is based on the number of ROIs, with each element ($A_{i,j}$) representing the connectivity between the respective regions.

Variable	Description	Band	Value
N	Number of dynamic connectivity matrices	Alpha	953
		Beta	1953
		Delta	226
		Gamma	3407
		Theta	544
n	Dimension of dynamic connectivity matrices	56×56	
$A_{i,j}$	Element of one connectivity matrix	–	

Specifically, for the alpha band, 953 matrices were created. Each matrix element $A_{i,j}$ represented the strength of the connections from node i to node j, referred to as an *edge* in graph theory-based analysis (Table 3).

BNS segmentation was performed on this dataset using a clustering algorithm to identify stable periods over time. The analysis was based on functions from the EEGLab Microstate toolbox, originally designed for EEG voltage topography. We adapted the microstate analysis pipeline described by Poulsen et al. to extract BNSs from functional connectivity data (Poulsen et al. 2018). The optimal number of classes was determined based on goodness-of-fit metrics, including Global Explained Variance (GEV) criterion (Murray et al. 2008; Poulsen et al. 2018).

For the clustering process, we transformed the symmetric connectivity matrices into vectors of size $(n \times (n-1)/2) = 1540$ by extracting the upper triangular elements, excluding the diagonal. Each vector was then concatenated across all time points, resulting in a subject-specific matrix of dimensions 1540×953, where each column represents a time window, and each row corresponds to a specific connection within the network. These matrices were concatenated among subjects and served as input for the modified k-means (k-means++) clustering algorithm (Pascual-Marqui et al. 1995), which has been successfully used in other previous studies on the dynamic functional connectivity of EEG and fMRI (Aubonnet et al. 2024; Zhu et al. 2023). Clustering was performed with the following parameters: the number of clusters varied from 2 to 10 (K_{range}), the number of random initializations (rep) was set to 100, and the maximum number of iterations (iter) was 1000, with a default convergence threshold of 10^{-6}.

A meta-criterion was applied to obtain the optimal number of clusters (Custo et al. 2017; Aubonnet et al. 2024; Mahini et al. 2022), which was determined to be six. Specifically, the meta-criterion was implemented using the CVIK Toolbox (José-García and Gómez-Flores 2023), a MATLAB framework that integrates 28 Cluster Validity Indices (e.g., Silhouette, Davies–Bouldin, Dunn, PBM, S_{Dbw}) and multiple proximity measures to automatically determine the optimal number of clusters based on index consensus.

Each identified cluster was defined as a BNS, representing the temporal evolution of brain connectivity. K-means++ was run multiple times with different parameters to ensure the robustness of the clustering results. The BNSs obtained from each clustering iteration were then compared using Pearson correlation analysis to assess the consistency of the identified patterns. A strong correlation indicated high similarity between BNSs across different clustering runs, validating the reliability of the extracted states (Table 4).

The topological visualization of the six BNSs was conducted, and they were labeled based on the most prevalent RSNs, as detailed in Subsection Data processing: Association of BNSs with RSNs. Each BNS was characterized by distinct spatial distributions and temporal dynamics that correspond to specific cognitive and functional processes. This allowed for a more intuitive interpretation of the BNSs in relation to established RSNs, facilitating comparisons between the two groups in our study.

As a final step, we computed the back-fitting at the subject level using Global Map Dissimilarity (GMD) to identify the best-fitting BNSs throughout the experiment. The smoothing process involved rejection based on small-segment criteria of five matrices (Aubonnet et al. 2023; Poulsen et al. 2018; Murray et al. 2008). For the identified BNSs, we calculated several common metrics used in microstate analysis, including Global Field Power (GFP), occurrence per second (occurrence), average duration (duration), percentage of time occupied (coverage), global explained variance (GEV), and the transition probabilities (TP). These metrics were subjected to statistical analysis between the

Table 4 Pearson correlation of the six Brain Network States across different clustering runs. The optimal number of clusters ($K = 6$) was determined using the meta-criterion based on multiple internal Cluster Validity Indices (CVIs). Modified k-means clustering was then repeated four times with different parameter configurations. Cluster #1, defined by the parameters $K_{\text{range}} = 2{:}10$, rep = 100, ite = 1000, was used as the reference for comparison. We therefore computed the Pearson correlation between the corresponding cluster maps obtained in different runs to evaluate the similarity and stability of the clustering results.

Clusters	Parameters	Pearson correlation					
		BNS1	BNS2	BNS3	BNS4	BNS5	BNS6
Cluster #2	K_{range}=2:10; rep=100; ite=1000	1	1	1	1	1	1
Cluster #3	K_{range}=3:7; rep=100; ite=1000	−1	1	0.99	0.99	0.99	1
Cluster #4	K_{range}=3:7; rep=200; ite=1000	1	1	1	0.99	0.99	1

two groups. A comprehensive description of these metrics is provided in Appendix Computational Methods for BNSs metrics.

Data Processing: Association of BNSs with RSNs

Each obtained BNS was computed from a vector to form a 56 $\times$ 56 symmetric matrix that represented the associated functional network. Based on some studies (Shirer et al. 2012; Kabbara et al. 2017), each of the 56 nodes was assigned to one of seven RSNs: Default Mode Network (DMN), Dorsal Attention Network (DAN), Salience Network (SAN), Motor Network (MOT), Auditory Network (AUD), Visual Network (VIS), and Other. The node-RSN affiliations are detailed in Appendix (ROI-Node-RSN Mapping). Using the Brain Connectivity Toolbox (Rubinov and Sporns 2010), the strength of each node was calculated, representing the sum of the weights of all links connected to that node. Subsequently, we determined the strength of each RSN by summing the values of nodes associated with the specific RSN and normalizing this sum by dividing it by the number of nodes within the RSN. To identify the dominant RSN for each BNS, we considered those with a value exceeding the sum of the average and standard deviation of the strengths of the seven RSNs. We utilized BrainNet Viewer (Xia et al. 2013) for visualization, where each ROI was represented by a color corresponding to its specific RSN. Each network was displayed with a sparsity of 0.01.

CorrelatioNs Between Questionnaire Scores and Brain State Metrics (Coverage, Occurrence, and Duration)

The study examined the relationships between coverage, duration, and occurrence variables derived from the BNS analysis of the PRE and POST phases, and the two indices, PHY and NEURO. Spearman correlation analysis was conducted to evaluate these relationships. Data were analyzed iteratively for each BNS and subject. Significant correlations ($p < 0.05$) indicated both linear and monotonic relationships across the data subsets.

Statistical Analysis

The statistical analysis was conducted to investigate the effects of the BNSs and subject group on occurrence, duration, and coverage across different phases of the experimental protocol. The study utilized a Linear Mixed Model (LMM) approach to account for the hierarchical structure of the data, where repeated measures within subjects were nested within the levels of the BNS factor. The primary objective was to ascertain any significant main effects and interactions between the subject group (PD vs. CTR) and the BNSs. Model fit was assessed by examining model summary statistics, including coefficients, standard errors, and p-values derived from likelihood ratio tests. Additionally, an analysis of variance (ANOVA) was performed to assess the overall significance of the fixed effects in the model. To further elucidate significant effects identified by the primary analysis, post-hoc pairwise comparisons were conducted using estimated marginal means. These comparisons aimed to delineate differences in the specific metrics between specific levels of the BNSs factor within each subject group across different experiment phases. To mitigate the risk of Type I errors arising from multiple pairwise comparisons, p-values were adjusted using the Benjamini-Hochberg method. This method controls the False Discovery Rate (FDR) and helps maintain the overall integrity of statistical inference. Results were visually represented through empirical cumulative distribution functions and pairs plots to illustrate the distributional properties of the data and highlight significant differences between experimental conditions.

Results

BNSs Presence

Following the back-fitting process, we initially identified distinct patterns in the presence of BNSs between individuals with PD and CTR subjects across the experimental phases (Fig. 3). All BNSs appeared in each phase for both cohorts, but their relative frequencies varied. Specifically, BNS1 was slightly more frequent in the PD group, except during the POST phase, where it was higher in the CTR group. The trend of BNS1 in the PD group remained consistent across all phases except for the POST phase, whereas in the CTR group, it differed in the PRE phase. BNS2 was consistently less frequent in the PD group across all phases. Conversely, BNS3 and BNS5 were consistently more prominent in the PD group. BNS4 was more frequent in the PD group except during the PRE phase, while BNS6 showed a higher presence in the CTR group except during the PRE phase.

CorrelatioNs Between Questionnaire Scores and Brain State Metrics

The correlation analysis between questionnaire indices and BNS metrics uncovered several significant relationships specific to BNS3. For the CTR group, a notable Spearman correlation was found between the occurrence metric and the NEURO index ($\rho = 0.27$, $p < 0.01$). Both groups showed significant correlations between NEURO scores and

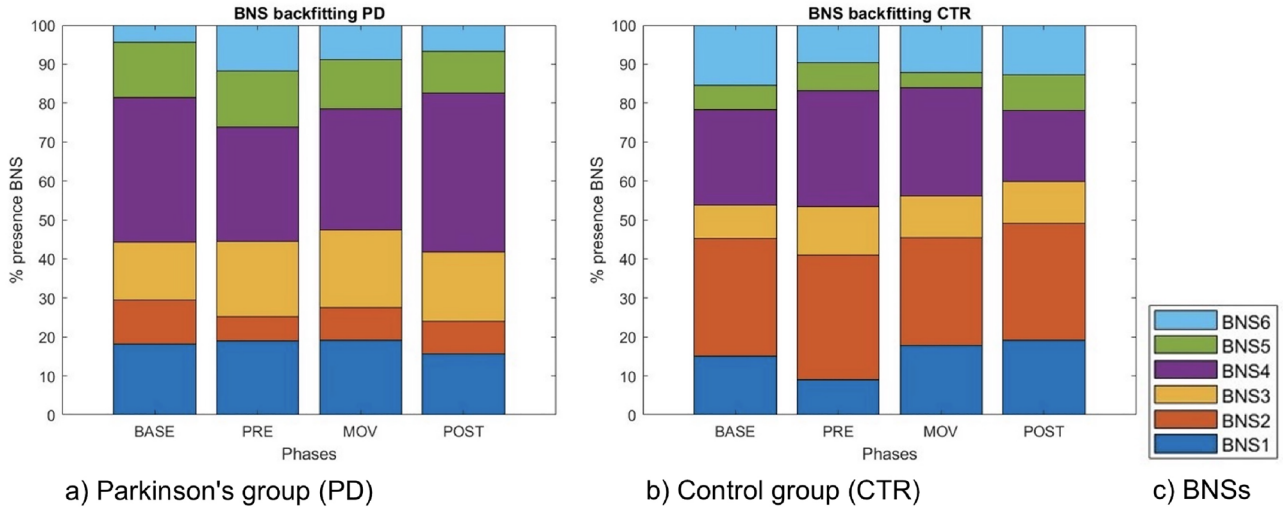

Fig. 3 Percentage representation of Brain Network States. Distribution of Brain Network States (BNSs) across different experimental time phases for (a) PD patients and (b) the CTR group. Each bar represents the frequency of a specific BNS during the respective phase, illustrating how often each state was engaged throughout the experiment. (c) Lists the identified BNSs

the metrics of coverage and duration within BNS3. In the CTR group, the correlation of duration with NEURO was $\rho = 0.24$ ($p < 0.02$), and for coverage, $\rho = 0.26$ ($p < 0.01$). Similarly, in the PD group, the duration-NEURO correlation was $\rho = 0.21$ ($p < 0.05$), and the coverage-NEURO correlation was $\rho = 0.22$ ($p < 0.05$). These findings indicated that both groups demonstrated significant associations between the NEURO index and the metrics of duration and coverage. However, the occurrence metric exhibited a unique correlation pattern that appeared only within the CTR group.

Statistical Analysis of BNSs

We investigated the following parameters of the BNSs: occurrence, duration, coverage, and TP. Statistical analysis revealed significant variations in BNS2 coverage during the PRE (adjusted p-value = 0.019) and MOV (adjusted p-value = 0.036) phases following FDR correction with $\alpha < 0.05$ (Fig. 4), consistent with an initial trend observed in these phases. For BNS4, a similar trend was observed in the BL and POST phases, although it did not remain significant after correction (Appendix Statistical Result of Coverage).

No statistically significant results were observed for occurrence; however, a trend was evident in BNS2 during the PRE and MOV phases (Appendix Statistical Result of Occurrence). For duration, no statistically significant results were found; however, a trend was noted in BNS5 during the BL phase and in BNS4 during the POST phase. TP analysis indicated that, in individuals with PD, transitions from BNS1 to BNS4 and from BNS4 to BNS1 consistently exhibited significantly higher probabilities compared to the CTR group. Conversely, transitions from BNS4 to BNS1 and BNS3 to BNS4 in CTR subjects displayed higher probabilities than those in the PD group starting from the PRE phase. In PD, activation within the same BNSs occurred later during the POST phase (Fig. 5, Appendix Statistical Result of Duration).

The statistical results findings are summarized in Table 5, which provides an overview of the main statistical outcomes for each BNS metric and experimental phase.

Association Between BNSs and RSNs

In Fig. 6, only the nodes were displayed, where the size of each node represented its strength, corresponding to the overall connectivity at that node. For visualization purposes, a sparsity threshold of 0.01 was applied, displaying only the strongest connections. This approach highlighted the most significant interactions, using color-coding to distinguish different RSNs. In BNS1, the VIS predominated, with nodes concentrated in the left hemisphere, particularly in the parietal and occipital lobes. The SAN was also prominent, with nodes distributed across the frontal and right parietal lobes. In the remaining five BNSs, the DAN was the dominant RSN. BNS2 featured the DAN primarily in the parietal lobe, with nodes of similar sizes spread across the interhemispheric fissure, followed by the SAN in the frontal lobe. BNS3 included the DMN in the frontal lobe, with balanced node strength between the left and right hemispheres, and the AUD in the parietal lobe. BNS4 comprised the DMN, with node strength balanced across the interhemispheric fissure in the parietal lobe, while being exclusively present in the right hemisphere in the frontal lobe. Additionally, the VIS network was mainly localized

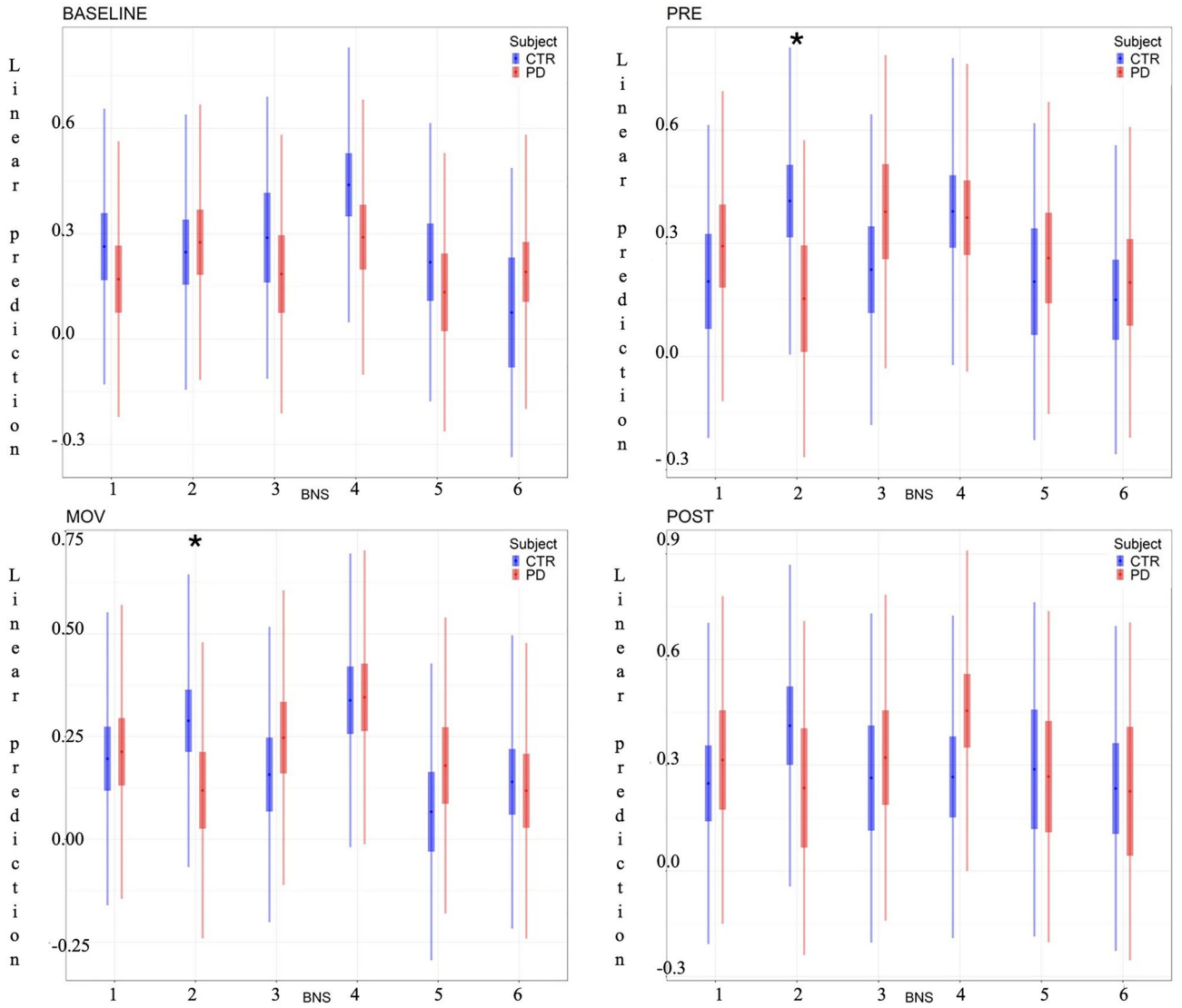

Fig. 4 Linear Mixed Model analysis. Coverage for each Brain Network States (BNSs) across all experimental phases in PD patients and CTR. Coverage refers to the proportion of total activity distributed across the six identified BNSs, indicating how dominant each BNS was relative to the others during each phase. Significant differences between groups, corrected using the False Discovery Rate (FDR) method, are highlighted: * $p < 0.05$.

in the left occipital lobe for the BNS4. BNS5 was similar to BNS4, with larger node sizes across the interhemispheric fissure and in the frontal lobe for the DAN, whereas the SAN was present in both hemispheres across the interhemispheric fissure. Finally, BNS6 involved both the DMN and the SAN, similar to BNS5, but with the DMN absent in the right hemisphere of the parietal lobe.

Discussion

This study examined brain dynamics during a complex PC task using the BioVRSea paradigm in early-stage PD patients. The novelty of this research lies in its visuomotor stimulation approach, which integrates VR and EEG to investigate motor-cognitive interactions in PD. This allowed for a detailed evaluation of PC impairments and their neural basis. To uncover brain network dynamics, we applied an innovative method adapted from the approach proposed by Poulsen et al. for extracting BNSs from functional connectivity data (Poulsen et al. 2018). This process included the selection of a clustering algorithm, BNS optimization, and back-fitting to derive key metrics such as coverage, occurrence, and duration. By analyzing BNSs within the specific BioVRSea paradigm, we aimed to identify new neurophysiological markers of PD that could aid in early diagnosis.

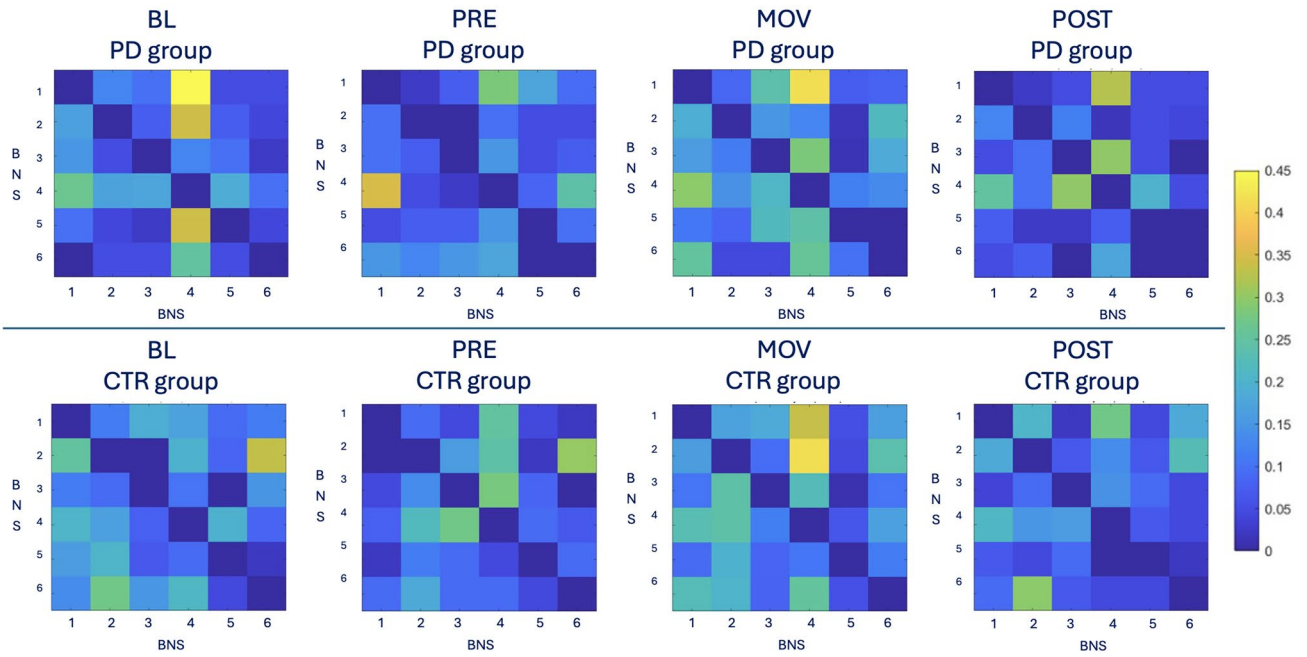

Fig. 5 Transition Probability matrices. PD and CTR subjects across baseline (BL), pre-motor stimulus (PRE), movement-stimulus (MOV), and post-motor stimulus (POST) phases. Each heatmap represents the likelihood of transitioning between different Brain Network States (BNSs) within each phase, with lighter colors indicating higher transition probabilities. These matrices highlight the patterns of state transitions and the differences between groups in terms of network dynamics

Table 5 Summary of main statistical outcomes for each Brain Network States metric and experimental phase. Linear Mixed Model (LMM) analysis with False Discovery Rate (FDR) correction ($\alpha < 0.05$). Significant results are highlighted in bold, while non-significant trends are also indicated for clarity.

Metric	Phase	BNS	Group difference (PD vs. CTR)	Adjusted p-value
Coverage	PRE	BNS2	PD < CTR	**0.019**
Coverage	MOV	BNS2	PD < CTR	**0.036**
Coverage	BL	BNS4	PD > CTR	n.s.
Coverage	POST	BNS4	PD > CTR	n.s.
Occurrence	PRE	BNS2	CTR > PD	n.s.
Occurrence	MOV	BNS2	CTR > PD	n.s.
Duration	BL	BNS5	PD > CTR	n.s.
Duration	POST	BNS4	CTR > PD	n.s.

BNS-Transition Probability Patterns

Across all phases, both groups showed similar transition structures, with only subtle differences in how the brain network states evolved over time. Control participants tended to display slightly more distributed transitions, suggesting a somewhat more flexible configuration of functional dynamics, while PD patients exhibited a modest tendency toward recurrent exchanges within a narrower subset of states. The most noticeable contrasts involved the transitions between BNS1↔BNS4 and BNS3↔BNS4, which appeared more pronounced in PD patients, particularly during task-related phases. However, these differences were not consistent across conditions and did not define a stable pattern distinguishing the two groups. Overall, the analysis did not reveal any clear or phase-specific transition pattern that could distinctly separate PD from CTR. Rather, group differences appeared as a general tendency for PD patients to show less flexible and more repetitive state transitions, instead of distinct or stable transition pathways.

BNS-Specific Analysis

BNSs and RSNs reflected patterns of functional connectivity between different brain regions. While RSNs were typically observed during rest, BNSs represented brain network configurations that occurred during various cognitive tasks or conditions. BNSs involved brain regions that were part of well-known RSNs, such as the default mode network or the fronto-parietal network. The brain states identified through EEG corresponded to RSNs observed in the resting-state. This suggested that certain brain regions remained functionally connected both during rest and while engaging in active tasks. The difference between the presence of RSNs and BNSs in PD compared to CTR referred to alterations in brain connectivity patterns observed in these two groups. This demonstrated altered connectivity and reduced dynamic flexibility of brain networks, reflecting difficulties in adapting to cognitive tasks and changing conditions, and highlighted the cognitive and motor impairments

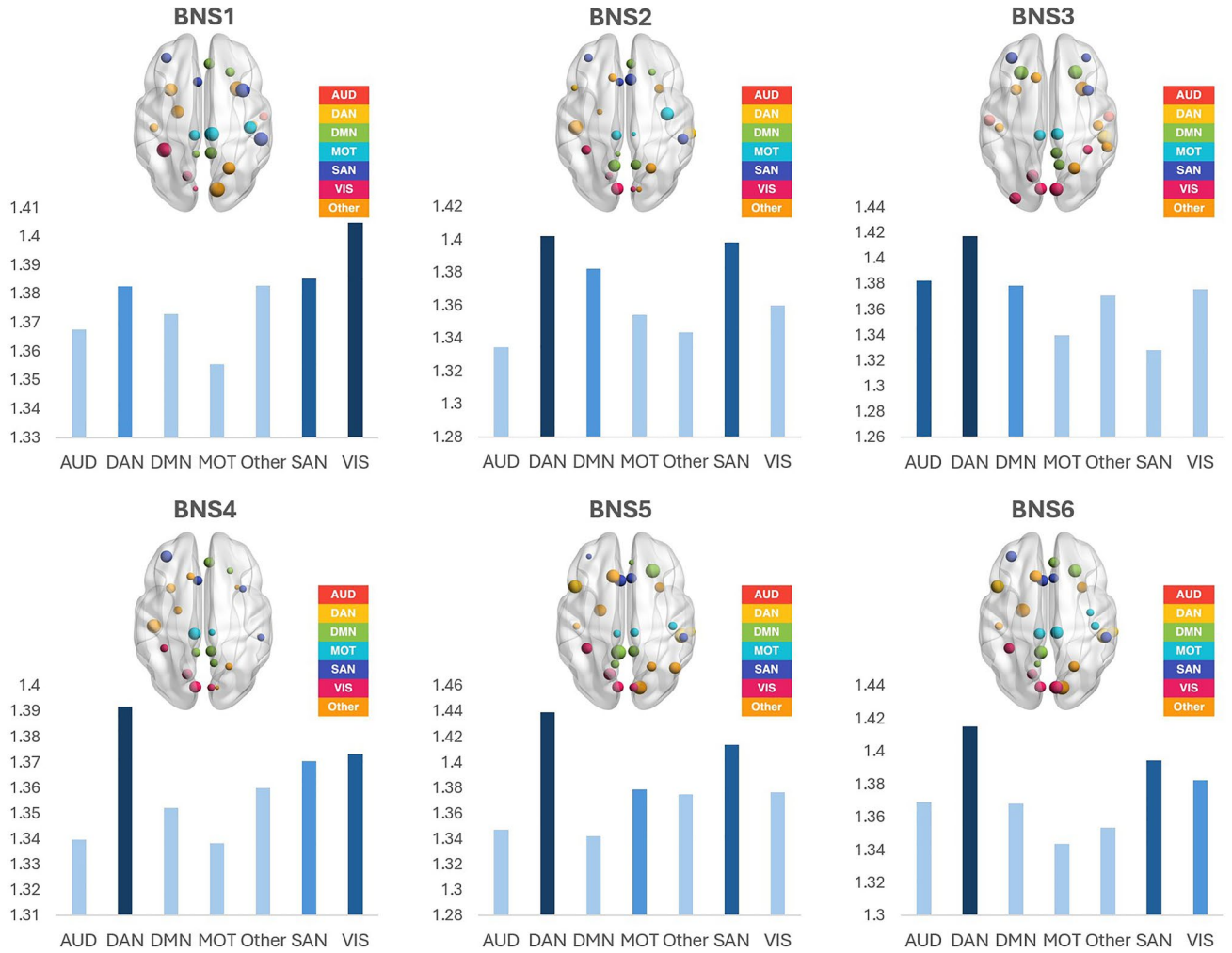

Fig. 6 Prevalence of Resting Network States in each Brain Network State. Calculated as the sum of the node strength values for each Region of interest (ROI) associated with the specific Resting Network State (RSNs). Each Brain Network State (BNS) is visualized with nodes sized proportionally to their strength (the sum of connections at each node), and edges are shown based on their connectivity, with a sparsity threshold of 0.01 applied to filter weak connections. Different colors represent distinct RSNs, facilitating clear visual differentiation of the dominant networks in each BNS. This visualization highlights the key RSNs contributing to the overall network dynamics across experimental phases

associated with the disease. **BNS1:** BNS1 showed a similar trend in PD compared to CTR, with the only difference in the PRE phase, where the visual stimulation began. Within BioVRSea, BNS1 had the VIS and SAN as its prevalent RSNs (Figs. 3, 6). The VIS comprised the primary visual cortex (V1) in the striate cortex (Brodmann area 17) and multiple extra-striate regions in the occipital lobe. Together, they covered a significant portion of the posterior cortical surface. This network was essential for processing visual information and played roles in object recognition, motion perception, and spatial awareness tasks. Understanding VIS helped to comprehend visual perception and cognition and to develop treatments for visual disorders and neurological conditions that affect vision (Seitzman et al. 2019; Fox et al. 2005; Beckmann et al. 2005). A study by Yao et al. identified significant differences in occipital function between PD patients without visual hallucinations (PDnonVH) and CTR subjects (Yao et al. 2015; Hsu et al. 2017; Hu et al. 2020). The PDnonVH group exhibited a lower amplitude of low-frequency fluctuations (ALFF) in the occipito-parietal region, indicating a reduced intrinsic activity in primary and associative visual areas. Additionally, PDnonVH patients showed decreased occipital functional connectivity with other brain regions, suggesting impaired visual processing and integration. The role of VIS and SAN in BNS1 could be more explicitly linked to maintaining alertness and responding to visual and motion cues within BioVRSea. During the PRE phase, when visual stimulation began, SAN activation likely represented participants' initial engagement with the immersive VR environment, preparing them for the motor challenge introduced in the MOV phase. Highlighting how VIS and SAN networks aligned with BioVRSea task

requirements provided important context to their prevalence in BNS1, reflecting the overall cognitive load imposed by the simulated environment in each phase.

BNS2: BNS2 was more prevalent in the CTR cohort (Fig. 3), with a notable presence of the DAN and SAN as its primary RSNs (Fig. 6). Recent research showed decreased DAN and SAN in PD patients (Vossel et al. 2014; Hsu et al. 2012). As shown in Fig. 6, the DAN was prevalent in the rest of five BNSs. This network was prominent in the brain, primarily consisting of regions that activated during goal-directed tasks. When a specific task or goal was the focus, the DAN directed attention accordingly. It was crucial in tasks requiring sustained attention and cognitive control (Seitzman et al. 2019; Corbetta and Shulman 2008). Specifically, the DAN was involved in the voluntary deployment of attention, guiding the allocation of attention to specific locations or objects in a top-down manner. In the BioVRSea paradigm, which involved dynamic visual and motor challenges, DAN activation helped participants concentrate on specific postural adjustments to maintain balance, especially under VR conditions where immersive, shifting visuals demanded constant recalibration. In PD, studies indicated that there was a lower percentage of significant connections and reduced connection strength within the DAN compared to controls (Vossel et al. 2014; Maidan et al. 2019; Fox et al. 2006). This diminished presence of BNS2 in PD participants may, therefore, indicate attentional deficits that hindered PC, suggesting that they might have struggled to maintain the sustained focus required by BioVRSea. The SAN was mainly located in the anterior cingulate cortex and played an essential role in vigilance and in responding to salient stimuli. In the context of BioVRSea, SAN likely supported participants' alertness to continuous visual stimuli essential for timely postural responses. The lower SAN activation observed in PD may have indicated a compromised arousal system, limiting the ability of PD patients to stay fully alert in the demanding VR environment (Seitzman et al. 2019; Menon and Uddin 2015; Sridharan et al. 2008). Overall, the involvement of both the DAN and SAN in BNS2 highlighted how BioVRSea tasks required attentional focus and responsiveness, underscoring the mental effort these tasks demanded, particularly for PD participants.

BNS3: BNS3 was strongly associated with the DAN and the AUD (Fig. 6). These networks played an essential role in integrating sensory information, which explained the significance of BNS3 in the PD group (Fig. 3). The AUD was involved in processing sound stimuli, including inputs from the primary auditory cortex (A1) and peripheral regions like the insula and superior temporal gyrus (Seitzman et al. 2019; Hackett et al. 2001). In BioVRSea, both visual and auditory inputs challenged balance, making the integration of these sensory cues vital for task performance. In the PD group, the activation of BNS3 reflected a need for intensified sensory integration to compensate for potential deficits in PC. The VR environment incorporated simultaneous visual and auditory stimuli, requiring participants to synchronize these inputs to maintain balance effectively. The presence of both the DAN and AUD in BNS3 emphasized the demand imposed by BioVRSea for attention to and processing multiple sensory inputs. This dynamic integration was particularly significant in PD, as patients may have relied more heavily on compensatory strategies, utilizing auditory and visual feedback to counterbalance sensory integration deficits in dynamic tasks (Seitzman et al. 2019; Raij et al. 2000; Gander et al. 2019).

BNS4: A higher percentage of BNS4 was observed in the PD cohort, with a prevalence of the DAN and VIS as RSNs (Fig. 3, Fig. 6). Like BNS1, it engaged the VIS, SAN, and DAN to initiate and maintain attention and awareness in response to early visual stimuli. BNS4 higher activation in the PD group indicated a sustained compensatory reliance on visual processing for spatial orientation as the task progressed. In the BioVRSea environment, this reliance on DAN and VIS in BNS4 could reflect PD participants' efforts to maintain postural stability through continuous visual feedback, as they may find it more challenging to integrate other sensory signals effectively.

BNS5 and BNS6: BNS5 showed a higher percentage in the PD cohort, characterized by the DAN and SAN as RSNs, whereas BNS6 was more prevalent in the CTR cohort, featuring the DAN and SAN as RSNs (Fig. 3, Fig. 6). In the BioVRSea setting, these networks were crucial for maintaining attention, alertness, and responding to task-relevant stimuli-key elements for balancing in a dynamic visual setting. The study by Putcha et al. suggested that in healthy individuals, the SAN and DMN were anti-correlated, meaning that SAN activation reduced DMN activity and vice versa (Putcha et al. 2016). This balance was disrupted in PD, where SAN dysfunction, likely due to striatal impairments, affected the ability to suppress DMN effectively (Putcha et al. 2016; Menon 2011). In the context of BioVRSea, where cognitive control and postural adjustments were continually required, this disrupted SAN-DMN coupling in PD may have led to less efficient cognitive responses and adaptive control. As a result, the typical anti-correlation seen in healthy individuals may have become a positive or less negative correlation in PD patients. This altered coupling between SAN and DMN in PD was linked to cognitive deficits commonly observed in the disease (Putcha et al. 2016, 2014). The increased presence of BNS5 in the PD group likely reflected a compensatory mechanism, wherein PD participants relied more on SAN and DAN activation to maintain attentiveness and actively process stimuli during the VR task. In contrast, the prevalence of BNS6 in the CTR

group, also involving SAN and DAN but without the same dysfunctional SAN-DMN interaction, might have supported more fluid cognitive control and attention shifts, aligning with the natural neural dynamics of healthy participants during the task. The primary role of DMN involved inward-focused cognitive processes at rest rather than engagement in task-related activities, explaining why it was not identified as primary during the BioVRSea task (Buckner et al. 2008; Andrews-Hanna et al. 2010). Since the experiment required sustained attention and responsiveness to external stimuli, the DMN did not play a central role. However, PD patients' disrupted SAN-DMN interaction could have affected how effectively they suppressed inward-focused thoughts, impacting their cognitive control and task performance in the BioVRSea challenging VR setup.

In summary, the shifts and interactions of the different brain network dynamics highlighted the impact of the disease on cognitive function. The coverage parameter indicated that BNS2 was significantly lower in PD compared to CTR in the two phases of visual and visuomotor tasks (PRE and MOV, respectively), as shown in Fig. 4.

Neurophysiological Differences in BNSs

The correlation analysis provided valuable insights into the neurophysiological effects of PD related to the specific BNS3. This network was associated with the AUD and the DAN. The analysis showed that occurrence is significantly linked to the neurological index (NEURO) from the BioVRSea questionnaire only in the CTR group. However, both groups demonstrated meaningful relationships between duration and coverage with NEURO. This suggests that individuals with PD may exhibit unusual brain activity patterns as they try to manage cognitive challenges. Increased activity in these brain networks might reflect how PD patients perceive their neurophysiological state, potentially indicating higher levels of stress or fatigue, which can negatively impact their quality of life. Overall, the relationships between BNS3 and the activity in AUD and DAN highlighted the neurophysiological changes observed in PD patients, as well as the brain compensatory responses in attention and cognition. The information extracted from the questionnaire can provide valuable insights, particularly regarding neurodegenerative diseases that affect balance and PC. Understanding these symptoms and their correlation with brain networks may assist in developing targeted interventions aimed at improving the overall well-being of patients.

Implications of BNSs in PC Task and in PD

These findings highlighted altered BNS dynamics in PD patients, particularly decreased BNS2 coverage (Fig. 4) and modified transition patterns between BNSs (Fig. 5). These alterations reflected deficits in attention, sensory integration, and network flexibility, all of which were essential for successful balance during dynamic tasks. The reduced BNS2 activity in PD patients during visuomotor phases suggested impaired attention and motor integration, while the increased reliance on visual processing networks (BNS4) underscored compensatory strategies in response to these deficits. The transition probability analysis further revealed PD-specific challenges in switching between states, particularly in moving between attentional (BNS1 and BNS4) and sensory-integration states, which may have contributed to PC deficits (Fig. 5).

Clinical Relevance

The BioVRSea paradigm researched quantitative metrics to evaluate the early onset of PD. The ultimate goal was to identify the most significant features that could be implemented using simple paradigms suitable for clinical settings. In neurological diseases like PD, the EEG framework used in this study helped identify key brain dysfunctions during balance tasks, especially in sensorimotor and cognitive networks. The EEG analysis could also detect neural changes linked to PD that might not yet have shown up in motor behavior. By examining BNSs from EEG data, clinicians were able to track changes in brain connectivity that reflected problems with PC, providing early signs of PD and allowing for diagnosis and intervention. The BioVRSea paradigm, combined with brain network analysis, helped develop more tailored treatment plans for PD patients.

Conclusion

This study aimed to use brain dynamics as a tool to identify new biomarkers for detecting neural dysfunction in early-stage PD, especially during our complex PC task. The proposed approach was a robust methodology that utilized functional connectivity to identify specific BNSs that alternated during the required tasks. By analyzing the differences with healthy individuals, this study intended to uncover neural changes associated with PD that might not have been visible using traditional methods. The study confirmed the effectiveness of the BioVRSea paradigm in exploring the mechanisms of PC. The visual-motor stimuli required the brain to adjust its physiological responses to regulate body position, and the rapid changes in brain activity evidenced

this adjustment. The advanced EEG analysis and clustering algorithms identified six distinct BNSs, with the DAN most active in five states, highlighting its role in behavioral performance and adaptation during attention-demanding tasks. The BNSs distribution on the subject level showed some differences in the BioVRSea phases. Notably, BNS2 coverage was significantly lower in PD patients during the visual and visuomotor phases, suggesting specific deficits in the neural mechanisms underlying PC at this particular stage of the disease, particularly in the brain regions associated with attention and sensory-motor integration. The focused analysis of alpha band activity revealed significant correlations with PC strategies associated with balance maintenance and postural adjustments. PD patients exhibited altered alpha band dynamics, highlighting potential biomarkers for early diagnosis and intervention. Furthermore, by prioritizing connectivity metrics over conventional channel-based approaches, this study provided a more comprehensive understanding of the neural processes involved in PC. The integration of graph theory allowed a detailed exploration of functional connectivity and its impact on PC. These findings underscore the potential of BNS dynamics as a diagnostic tool for identifying neural deficits in PD and other neurological disorders. The BioVRSea paradigm and advanced EEG analysis offered a promising approach for developing targeted interventions to improve postural stability in affected individuals. Overall, this study advanced our understanding of brain connectivity dynamics in PC tasks and highlighted the importance of alpha band activity in maintaining balance. The innovative methodologies and findings paved the way for future research and clinical applications to enhance the quality of life for individuals with neural-motor impairments.

Limitations

In the present manuscript, we focused on the alpha band, conducting a deeper analysis based on previous findings obtained using the BioVRSea setup in Parkinson's disease patients (Jacob et al. 2022a), which demonstrated significant alterations in this frequency range and highlighted its strong involvement in postural control and visuomotor integration. The alpha band, therefore, represents a robust starting point for exploring functional connectivity in this population, being closely linked to cortical idling and inhibitory control-two mechanisms particularly relevant to our experimental paradigm. Importantly, the present work constitutes a preliminary investigation and the first application of the BioVRSea paradigm to a neurodegenerative cohort using EEG-based connectivity analysis, aiming to characterize the dynamic reorganization of brain networks during a realistic postural control task. However, we recognize that by focusing exclusively on the alpha band, potential insights from other frequency ranges may not have been captured. In particular, beta oscillations, which are strongly implicated in motor control, could reveal abnormal synchronization patterns in PD during movement anticipation or stabilization, providing a closer link between network rigidity and clinical motor symptoms such as bradykinesia or postural stiffness (Heinrichs-Graham and Wilson 2013; Gulberti and colleagues 2024). Theta activity, on the other hand, is associated with cognitive control, error monitoring, and sensorimotor integration, and might shed light on the interplay between attention and balance maintenance, especially under challenging sensory conditions (Miladinović and colleagues 2021; Anjum and colleagues 2024). Finally, delta oscillations could reflect large-scale coordination and compensatory processes supporting postural stability when cortical demand increases due to sensory conflict or fatigue (Singh and colleagues 2023).

Integrating these frequency-specific dynamics would thus help to clarify the contributions of motor, cognitive, and compensatory mechanisms to postural control deficits in PD. Future work will extend the present framework to these bands, combining them with the dynamic network analysis implemented here to obtain a more comprehensive, multi-frequency characterization of cortical network reorganization in Parkinson's disease.

It is important to note that several methodological alternatives exist for both source reconstruction and the computation of connectivity matrices. These steps can be implemented using different approaches, and no universally accepted gold standard currently exists. The combination of wMNE and PLV has demonstrated superior performance during cognitive tasks (Hassan et al. 2014). Specifically, Hassan et al. conducted a systematic comparison of multiple inverse and connectivity method combinations and showed that wMNE combined with PLV provided the best performance in identifying networks topologically consistent with known functional brain architectures. Dynamic connectivity within the BioVRSea paradigm was also analyzed in a cohort of healthy participants and published by Aubonnet et al. (Aubonnet et al. 2023), where the wMNE–PLV approach successfully captured meaningful brain network dynamics in the alpha band during complex postural control tasks.

Appendix A: ROI-Node-RSN Mapping

see Table 6.

Table 6 Regions of Interest (ROIs) and their Functional Network Associations

ROI	Label	Acronym	RSN	ROI	Label	Acronym	RSN
1	l.bankssts	l.BSTS	Other	29	l.middletemporal	l.MTG	DAN
2	r.bankssts	r.BSTS	Other	30	r.middletemporal	r.MTG	DAN
3	l.cACC	l.cACC	SAN	31	l.paracentral	l.paraC	MOT
4	r.cACC	r.cACC	SAN	32	r.paracentral	r.paraC	MOT
5	l.cMFG	l.cMFG	SAN	33	l.pericalcarine	l.periCAL	Other
6	r.cMFG	r.cMFG	SAN	34	r.pericalcarine	r.periCAL	Other
7	l.cuneus	l.CUN	VIS	35	l.postcentral	l.postC	MOT
8	r.cuneus	r.CUN	VIS	36	r.postcentral	r.postC	MOT
9	l.entorhinal	l.ENT	Other	37	l.posteriorcingulate	l.PCC	DMN
10	r.entorhinal	r.ENT	Other	38	r.posteriorcingulate	r.PCC	DMN
11	l.superiorfrontal	l.sFG	Other	39	l.precentral	l.preC	MOT
12	r.superiorfrontal	r.sFG	Other	40	r.precentral	r.preC	MOT
13	l.fusiform	l.FUS	VIS	41	l.precuneus	l.PCUN	DMN
14	r.fusiform	r.FUS	VIS	42	r.precuneus	r.PCUN	DMN
15	l.inferiorparietal	l.IPL	Other	43	l.rACC	l.rACC	DMN
16	r.inferiorparietal	r.IPL	Other	44	r.rACC	r.rACC	DMN
17	l.ITG	l.ITG	DAN	45	l.rMFG	l.rMFG	SAN
18	r.ITG	r.ITG	DAN	46	r.rMFG	r.rMFG	SAN
19	l.pOPER	l.pOPER	DAN	47	l.SPL	l.SPL	Other
20	r.pOPER	r.OPER	DAN	48	r.SPL	r.SPL	Other
21	l.isthmuscingulate	l.iCC	DMN	49	l.STG	l.STG	AUD
22	r.isthmuscingulate	r.iCC	DMN	50	r.STG	r.STG	AUD
23	l.lateraloccipital	l.LOG	VIS	51	l.SMAR	l.SMAR	SAN
24	r.lateraloccipital	r.LOG	VIS	52	r.SMAR	r.SMAR	SAN
25	l.LOF	l.LOF	DMN	53	l.TP	l.TP	Other
26	r.LOF	r.LOF	DMN	54	r.TP	r.TP	Other
27	l.LING	l.LING	VIS	55	l.TT	l.TT	Other
28	r.LING	r.LING	VIS	56	r.TT	r.TT	Other

Appendix B: Phase-Locking Value (PLV) Calculation

The dynamic Phase-Locking Value (PLV) dynamic connectivity matrices are computed using the function:

$$\boxed{N = \left\lfloor \frac{Numberof Samples - OverlapWindow}{TotalWindow - OverlapWindow} \right\rfloor}$$

where:

$$\begin{cases} \text{NumberofSamples} &= \text{EpochDuration} \times \text{SamplingRate} \\ f_{\text{Interest}} &= f_{\min} + \frac{(f_{\max} - f_{\min})}{2} \\ \text{TotalWindow} &= \left\lfloor \frac{6}{f_{\text{Interest}}} \times \text{SamplingRate} \right\rfloor \\ \text{OverlapWindow} &= \left\lfloor \frac{\text{OverlapPercentage}}{100} \times \frac{6}{f_{\text{Interest}}} \times \text{SamplingRate} \right\rfloor \end{cases}$$

This function takes as input:

- *EpochDuration*: EEG time series with dimensions $[n_{\text{channels}}, n_{\text{samples}}]$.
- *SamplingRate*: The EEG sampling frequency.
- *fmin*, *fmax*: The lower and upper-frequency limits of the band of interest.
- *OverlapPercentage*: The percentage of overlap between time windows.The number of dynamic matrices (N) generated for each frequency band depends on the *length* of each analysis window and on the *overlap* between consecutive windows. Following (Lachaux et al. 2000), each window spans six cycles of the band's center frequency to ensure reliable phase estimation.

In our implementation, the *Epoch Duration* was 273 s, the *Sampling Rate* was 1024 Hz, and the *Overlap Percentage* between consecutive windows was set to 50%, providing a balance between temporal resolution and the stability of the phase-locking estimates.

Band	**Frequency parameters (Hz)**			**Window parameters (samples)**		
	$f_{\min}$	$f_{\max}$	f_{Interest}	TotalWindow (samples per segment)	OverlapWindow(samples shared)	N (PLV matrices)
Delta	1	4	2.50	2457	1228	226
Theta	4	8	6.00	1024	512	545
Alpha	**8**	**13**	**10.5**	**585**	**292**	**953**
Beta	13	30	21.5	285	142	1953
Gamma	30	45	37.5	163	81	3408

Example calculation for the alpha band:

Epoch Duration = 273 s; Sampling Rate = 1024 Hz; Overlap = 50%.

Number of Samples = $273 \times 1024 = 279552$ samples.

$f_{\min} = 8$ Hz; $f_{\max} = 13$ Hz $\Rightarrow f_{\text{Interest}} = 10.5$ Hz.

Total Window = $\lfloor 6/10.5 \times 1024 \rfloor = \lfloor 585.14 \rfloor = 585$ samples

Overlap Window = $\lfloor 0.5 \times 585.14 \rfloor = \lfloor 292.47 \rfloor = 292$ samples

$$N = \left\lfloor \frac{279552 - 292}{585 - 292} \right\rfloor = \left\lfloor \frac{279260}{293} \right\rfloor = \lfloor 953.10 \rfloor = 953.$$

Appendix C: Computational Methods for BNSs Metrics

See Table 7.

Table 7 Description of parameters used in the analysis of brain network states (BNSs), including their formulas and interpretations

Parameter	Formula	Description
Coverage	$\text{Coverage}_i = \frac{T_i}{T_{\text{total}}}$ where T_i is the total time state was active, and T_{total} is the total analysis time.	Coverage represents the proportion of time a BNS is active relative to the total time.
Duration	$\text{Duration}_i = \frac{T_i}{N_i}$ where T_i is the total time state was active, and N_i is the number of times state was activated.	Duration is the average time a BNS remains active before switching to another.
GEV	$\text{GEV}_i = \frac{\sum_{t \in i} \text{GFP}(t) \cdot \text{CC}(t)^2}{\sum_t \text{GFP}(t)}$ where $\text{GFP}(t)$ is the Global Field Power at time t, and $\text{CC}(t)$ is the spatial correlation between the map at time t and the template map of state .	GEV represents the proportion of the Global Field Power explained by each BNS, indicating how well each state represents the data.
GFP	$\text{GFP}(t) = \sqrt{\frac{1}{N} \sum_{i=1}^{N} \left(V_i(t) - \overline{V(t)}\right)^2}$ where $V_i(t)$ is the voltage at sensor at time t, $\overline{V(t)}$ is the mean voltage across all sensors, and N is the total number of sensors.	GFP quantifies the variance of the EEG signal at a given time point, providing a measure of the strength of brain activity.
GMD	$\text{GMD}(t) = \sqrt{\frac{1}{N} \sum_{i=1}^{N} \left(\frac{V_i(t)}{\sqrt{\sum_{i=1}^{N} V_i^2(t)}} - \frac{V_i(r)}{\sqrt{\sum_{i=1}^{N} V_i^2(r)}} \right)^2}$ where $V_i(t)$ and $V_i(r)$ are the voltages at sensor at times t and r, respectively, and N is the total number of sensors.	GMD quantifies the dissimilarity between two topographical voltage distributions over time.
Occurrence	$\text{Occurrence}_i = \frac{N_i}{T_{\text{total}}}$ where N_i is the number of times state was activated, and T_{total} is the total analysis time.	Occurrence measures how many times a specific BNS appears within a time window.
TP	$T_{ij} = \frac{N_{ij}}{\sum_j N_{ij}}$ where T_{ij} is the transition probability from state to state j, N_{ij} is the observed transitions from to j, and $\sum_j N_{ij}$ is the total transitions from to any state.	TP describes the probabilities of transitioning between different BNSs over time.

Appendix D: Statistical Result of Coverage

See Table 8.

Table 8 Coverage p-values and adjusted p-values after FDR correction for different BNSs across phases (BL, PRE, MOV, POST) in the CTR - PD contrast

BL Phase			PRE Phase			MOV Phase			POST Phase		
BNS	p-value	adjusted p-value	BNS	p-value	adjusted p-value	BNS	p-value	adjusted p-value	BNS	p-value	adjusted p-value
4	0.024	0.143	2	0.003	**0.019***	2	0.006	**0.036***	4	0.018	0.109
1	0.178	0.337	3	0.077	0.231	5	0.100	0.300	2	0.086	0.259
6	0.201	0.337	1	0.271	0.541	3	0.159	0.319	1	0.459	0.854
3	0.229	0.337	5	0.504	0.673	6	0.723	0.904	3	0.570	0.854
5	0.281	0.337	6	0.561	0.673	1	0.769	0.904	5	0.859	0.944
2	0.671	0.671	4	0.815	0.815	4	0.904	0.904	6	0.944	0.944

Appendix E: Statistical Result of Occurrence

See Table 9.

Table 9 Occurrence p-values and adjusted p-values after FDR correction for different BNSs across phases (BL, PRE, MOV, POST) in the CTR - PD contrast

BL Phase			PRE Phase			MOV Phase			POST Phase		
BNS	p-value	adjusted p-value	BNS	p-value	adjusted p-value	BNS	p-value	adjusted p-value	BNS	p-value	adjusted p-value
1	0.082	0.372	2	0.032	0.174	2	0.038	0.228	6	0.324	0.877
6	0.124	0.372	1	0.058	0.174	1	0.566	0.793	1	0.513	0.877
4	0.607	0.672	6	0.450	0.678	5	0.581	0.793	2	0.553	0.877
5	0.615	0.672	5	0.452	0.678	6	0.626	0.793	5	0.615	0.877
3	0.653	0.672	4	0.815	0.978	4	0.661	0.793	3	0.730	0.877
2	0.672	0.672	3	1.000	1.000	3	0.885	0.885	4	0.975	0.975

Appendix F: Statistical Result of Duration

See Table 10.

Table 10 Duration p-values and adjusted p-values after FDR correction for different BNSs across phases (BL, PRE, MOV, POST) in the CTR - PD contrast

BL Phase			PRE Phase			MOV Phase			POST Phase		
BNS	p-value	adjusted p-value	BNS	p-value	adjusted p-value	BNS	p-value	adjusted p-value	BNS	p-value	adjusted p-value
5	0.042	0.253	1	0.312	0.727	5	0.096	0.231	4	0.035	0.210
3	0.111	0.261	6	0.327	0.727	6	0.134	0.231	6	0.244	0.724
4	0.130	0.261	3	0.440	0.727	4	0.165	0.231	1	0.362	0.724
6	0.400	0.601	4	0.485	0.727	3	0.168	0.231	3	0.548	0.768
1	0.750	0.893	2	0.682	0.757	1	0.192	0.231	2	0.702	0.768
2	0.893	0.893	5	0.757	0.757	2	0.366	0.366	5	0.768	0.768

Acknowledgements The authors would like to thank the RANNIS, Icelandic Research Fund (Grant of Excellence no: 239612-051), and the research fund of Landspitali University Hospital.

Author Contributions Federica Pescaglia: Conceptualization, Data Curation, Formal Analysis, Investigation, Methodology, Software, Validation, Visualization, Writing – Original Draft Preparation, Writing – Review and Editing, Lorena Guerrini: Conceptualization, Data Curation, Formal Analysis, Investigation, Methodology, Software, Validation, Visualization, Writing – Original Draft Preparation, Writing – Review and Editing Carmine Gelormini: Formal Analysis, Investigation, Methodology Romain Aubonnet: Conceptualization, Investigation, Methodology, Resources, Supervision, Writing – Review and Editing Gylfi Örn Thormar: Resources Giorgio Di Lorenzo: Conceptualization, Data Curation, Formal Analysis, Supervision Halldór Jónsson jr: Resources, Writing – Review and Editing Mahmoud Hassan: Conceptualization, Methodology Paolo Gargiulo: Conceptualization, Formal Analysis, Funding Acquisition, Investigation, Methodology, Project Administration, Resources, Supervision, Validation, Writing – Review and Editing.

Funding Open access funding provided by Reykjavik University.

Data Availability The data are not publicly available due to privacy and ethical restrictions related to Parkinson's disease patients, but can be provided by the authors upon reasonable request.

Declarations

Competing interests The authors declare that there are no conflicts of interest regarding the publication of this paper. None of the authors has any financial or personal relationships that could be perceived as influencing the research outcomes or interpretations presented in this study.

Ethical Approval All procedures performed in studies involving human participants were in accordance with the ethical standards of the institutional and Icelandic national research committee and with the 1964 Helsinki Declaration and its later amendments or comparable ethical standards. The study protocol was approved by the Icelandic National Bioethics Committee with the consent no:VSN-20–101 for the recruitment and assessment of the healthy cohort and extended it to include the Parkinson's cohort under amendment no:VSN-20–101-V2.

Informed Consent All participants received detailed written notification about the study and provided their signed informed consent.

References

Ablin P, Cardoso JF, Gramfort A (2018) Faster ica under orthogonal constraint. 2018 IEEE International Conference on Acoustics. IEEE, Speech and Signal Processing (ICASSP), pp 4464–4468

Aljalal M, Aldosari SA, AlSharabi K et al (2022) Parkinson's disease detection from resting-state EEG signals using common spatial pattern, entropy, and machine learning techniques. Diagnostics 12(5):1033

Andrews-Hanna JR, Smallwood J, Spreng RN (2010) The default network and self-generated thought: component processes, dynamic control, and clinical relevance. Ann N Y Acad Sci 1316(1):29–52

Anjum A (2024) Resting-state EEG measures cognitive impairment in Parkinson's disease. NPJ Parkinsons Dis 10(1):1–10. https://doi.org/10.1038/s41531-023-00602-0

ANT Neuro (2023) Ant neuro academy faq. https://academy.ant-neuro.com/faq, accessed: 2025-01-17

Araújo-Silva F, Santinelli FB, Imaizumi LFI et al (2022) Temporal dynamics of cortical activity and postural control in response to the first levodopa dose of the day in people with Parkinson's disease. Brain Res 1775:147727

Aubonnet R, Shoykhet A, Jacob D et al (2022) Postural control paradigm (BioVRSea): towards a neurophysiological signature. Physiol Meas 43(11):115002

Aubonnet R, Hassan M, Mheich A et al (2023) Brain network dynamics in the alpha band during a complex postural control task. J Neural Eng 20(2):026030

Aubonnet R, Hassan M, Gargiulo P, et al (2024) Dynamic resting-state eeg alpha connectivity: Quantifying brain network state evolution in individuals with psychosis. bioRxiv, 2024–06

Balasubramaniam R, Wing AM (2002) The dynamics of standing balance. Trends Cogn Sci 6(12):531–536

Barollo F, Hassan M, Petersen H et al (2022) Cortical pathways during postural control: new insights from functional EEG source connectivity. IEEE Trans Neural Syst Rehabil Eng 30:72–84

Beckmann CF, DeLuca M, Devlin JT et al (2005) Investigations into resting-state connectivity using independent component analysis. Philos Trans R Soc Lond B Biol Sci 360(1457):1001–1013

Benamer HT, Patterson J, Grosset DG et al (2000) Accurate differentiation of parkinsonism and essential tremor using visual assessment of [123i]-fp-cit spect imaging: the [123i]-fp-cit study group. Mov Disord 15(3):503–510

Bhidayasiri R, Tarsy D, Bhidayasiri R (2012) Parkinson's disease: Hoehn and yahr scale. Movement disorders: a video atlas: a video atlas. pp 4–5

Brooks DJ (2010) Imaging approaches to parkinson disease. J Nucl Med 51(4):596–609

Buckner RL, Andrews-Hanna JR, Schacter DL (2008) The brain's default network: anatomy, function, and relevance to disease. Ann N Y Acad Sci 1124(1):1–38

Cohen MX (2015) Effects of time lag and frequency matching on phase-based connectivity. J Neurosci Methods 250:137–146

Corbetta M, Shulman GL (2008) The reorienting system of the human brain: from environment to theory of mind. Neuron 58(3):306–324

Custo A, Van De Ville D, Wells WM et al (2017) Electroencephalographic resting-state networks: source localization of microstates. Brain Connect 7(10):671–682

Del Din S, Godfrey A, Mazzà C et al (2016) Free-living monitoring of parkinson's disease: lessons from the field. Mov Disord 31(9):1293–1313

Del Percio C, Brancucci A, Bergami F et al (2007) Cortical alpha rhythms are correlated with body sway during quiet open-eyes standing in athletes: a high-resolution EEG study. Neuroimage 36(3):822–829

Desikan RS, Ségonne F, Fischl B et al (2006) An automated labeling system for subdividing the human cerebral cortex on MRI scans into gyral based regions of interest. Neuroimage 31(3):968–980

Doblhoff S, Friedl W (2018) Neuromuscular and cortical adaptations to postural control training. Neurosci Lett 671:64–70

Dos S, Santos H (2013) Cortical alpha oscillations predict postural sway modifications induced by transcranial direct current stimulation. Neurosci Lett 553:45–49

Edmunds KJ, Petersen H, Hassan M et al (2019) Cortical recruitment and functional dynamics in postural control adaptation and habituation during vibratory proprioceptive stimulation. J Neural Eng 16(2):026037

Farahibozorg SR, Henson RN, Hauk O (2018) Adaptive cortical parcellations for source reconstructed EEG/MEG connectomes. Neuroimage 169:23–45

Fox M, Corbetta M, Snyder A et al (2006) Spontaneous neuronal activity distinguishes human dorsal and ventral attention systems. Proc Natl Acad Sci USA 103(26):10046–10051

Fox MD, Raichle ME (2007) Spontaneous fluctuations in brain activity observed with functional magnetic resonance imaging. Nat Rev Neurosci 8(9):700–711

Fox MD, Snyder AZ, Vincent JL et al (2005) The human brain is intrinsically organized into dynamic, anticorrelated functional networks. Proc Natl Acad Sci U S A 102(27):9673–9678

Gander PE, Bosker HR, Teder-Sälejärvi WA et al (2019) Multimodal integration of visual and auditory information during speech perception. Hum. Brain Mapp. 40(13):3796–3809

Golding JF (2006) Predicting individual differences in motion sickness susceptibility by questionnaire. Pers Individ Differ 41(2):237–248

Gulberti A, colleagues, (2024) Premotor cortical beta synchronization and the network mechanisms of motor impairment in parkinson's disease. Neurobiology of Disea. https://doi.org/10.1016/j.nbd.2024.106259

Guttmann-Flury E, Wei Y, Zhao S, et al (2025) The cost of simplicity: How reducing eeg electrodes affects source localization and bci accuracy. arXiv preprint arXiv:2510.10770

Hackett TA, Preuss TM, Kaas JH (2001) Organization of the auditory cortex in humans and nonhuman primates: functional anatomy of the lateral auditory belt and parabelt. Prog Brain Res 130:273–288

Hassan M, Wendling F (2018) Electroencephalography source connectivity: aiming for high resolution of brain networks in time and space. IEEE Signal Process Mag 35(3):81–9

Hassan M, Dufor O, Merlet I et al (2014) EEG source connectivity analysis: from dense array recordings to brain networks. PLoS One 9(8):e105041

Hausdorff JM (2009) Gait dynamics in Parkinson's disease: common and distinct behavior among stride length, gait variability, and fractal-like scaling. Chaos Interdiscip J Nonlinear Sci. https://doi.org/10.1063/1.3147408

Heinrichs-Graham E, Wilson TW (2013) Neuromagnetic evidence of abnormal movement-related beta desynchronization in Parkinson's disease. Neuroimage Clin 2:585–59. https://doi.org/10.1016/j.nicl.2013.04.008

Hsu J, Ouyang C, Chen P et al (2017) Brain network alterations in patients with visual hallucinations in Parkinson's disease. J. Neurol. 264(7):1479–1489
Hsu W, Zanto T, Gazzaley A et al (2012) Functional connectivity of the dorsal attention network predicts post-stroke motor recovery. J. Neurosci. 32(21):7338–7343
Hu X, Zhang Y, Hu X et al (2020) Altered interhemispheric synchrony in Parkinson's disease patients with visual hallucinations: a resting-state fmri study. Cortex 124:201–210
Hülsdünker T, Mierau A, Neeb C et al (2015) Cortical processes associated with continuous balance control as revealed by EEG spectral power. Neurosci Lett 592:1–5
Jacob D, Aubonnet R, Recenti M et al (2022) Assessing early-stage Parkinson's disease using Biovrsea. 2022 IEEE International Conference on Metrology for Extended Reality. IEEE, Artificial Intelligence and Neural Engineering (MetroXRAINE), pp 271–276
Jacob D, Unnsteinsdóttir Kristensen IS, Aubonnet R et al (2022) Towards defining biomarkers to evaluate concussions using virtual reality and a moving platform (BioVRSea). Sci Rep 12(1):8996
Jacob D, Guerrini L, Pescaglia F et al (2023) Adaptation strategies and neurophysiological response in early-stage Parkinson's disease: BioVRSea approach. Front Hum Neurosci. https://doi.org/10.3389/fnhum.2023.1197142
José-García A, Gómez-Flores W (2023) Cvik: a matlab-based cluster validity index toolbox for automatic data clustering. SoftwX 22:101359
Kabbara A, El Falou W, Khalil M et al (2017) The dynamic functional core network of the human brain at rest. Sci Rep 7(1):2936
Kabbara A, Paban V, Hassan M (2021) The dynamic modular fingerprints of the human brain at rest. Neuroimage 227:117674
Kelly V, Johnson C, McGough E et al (2015) Association of cognitive domains with postural instability/gait disturbance in Parkinson's disease. Parkinsonism Relat Disord 21(7):692–697
Kilzheimer A, Hentrich T, Burkhardt S et al (2019) The challenge and opportunity to diagnose parkinson's disease in midlife. Front Neurol 10:1328
Kothe CAE, Jung TP (2016) Artifact removal techniques with signal reconstruction. 6th International BCI Meeting US Patent App. 14/895,440
Lachaux JP, Rodriguez E, Le Van QM et al (2000) Studying single-trials of phase synchronous activity in the brain. International Journal of Bifurcation and Chaos 10(10):2429–2439
Lanthier J, Simoneau M, Knoth IS et al (2020) Increased EEG alpha peak frequency in adolescents with idiopathic scoliosis during balance control in normal upright standing. Neurosci Lett 722:134836
Lopes MA, Junges L, Tait L et al (2020) Computational modelling in source space from scalp eeg to inform presurgical evaluation of epilepsy. Clin Neurophysiol 131(1):225–234
Lv H, Wang Z, Tong E et al (2018) Resting-state functional mri: everything that nonexperts have always wanted to know. Am. J. Neuroradiol. 39(8):1390–1399
Ma L, Marshall PJ, Wright WG (2022) The impact of external and internal focus of attention on visual dependence and EEG alpha oscillations during postural control. J Neuroeng Rehabil 19(1):81
Mahini R, Xu P, Chen G et al (2022) Optimal number of clusters by measuring similarity among topographies for spatio-temporal erp analysis. Brain Topogr 35(5):537–557
Maidan I, Jacob Y, Giladi N et al (2019) Altered organization of the dorsal attention network is associated with freezing of gait in Parkinson's disease. Parkinsonism Relat Disord 63:77–82
Mancini M, Horak FB (2010) The relevance of clinical balance assessment tools to differentiate balance deficits. Eur J Phys Rehabil Med 46(2):239
Menon V (2011) The triple network model of psychopathology: evidence from intrinsic functional connectivity and task effects. Biol Psychiat 69(12):1178–1185
Menon V, Uddin L (2015) Saliency, switching, attention and control: a network model of insula function. Brain Struct Funct 214(5–6):655–667
Miladinović A, colleagues (2021) Eeg changes and motor deficits in parkinson's disease patients: Correlation of motor scales and eeg power bands. arXiv preprint https://arxiv.org/abs/2106.02387,
Molcho L, Maimon NB, Hezi N et al (2023) Evaluation of Parkinson's disease early diagnosis using single-channel EEG features and auditory cognitive assessment. Front Neurol 14:1273458
Morris M, Iansek R, McGinley J et al (2005) Three-dimensional gait biomechanics in Parkinson's disease: evidence for a centrally mediated amplitude regulation disorder. Mov Disord 20(1):40–50
Mulert C (2013) Simultaneous EEG and fMRI: towards the characterization of structure and dynamics of brain networks. Dialogues Clin Neurosci 15(3):381–386
Murray MM, Brunet D, Michel CM (2008) Topographic ERP analyses: a step-by-step tutorial review. Brain Topogr 20(4):249–264
Niedermeyer E, da Silva FL (2005) Electroencephalography: basic principles, clinical applications, and related fields. Lippincott Williams & Wilkins
Pascual-Marqui RD, Michel CM, Lehmann D (1995) Segmentation of brain electrical activity into microstates: model estimation and validation. IEEE Trans Biomed Eng 42(7):658–665
Petersen SE, Sporns O (2015) Brain networks and cognitive architectures. Neuron 88(1):207–219
Poulsen AT, Pedroni A, Langer N, et al (2018) Microstate EEGlab toolbox: An introductory guide. BioRxiv p 289850
Priplata AA, Niemi JB, Harry JD et al (2003) Vibrating insoles and balance control in elderly people. Lancet 362(9390):1123–1124
Putcha D, Ross RS, Cronin-Golomb A et al (2014) Default network connectivity and cognition in Parkinson's disease. Hum. Brain Mapp. 35(9):4018–4031
Putcha D, Ross RS, Cronin-Golomb A et al (2016) Salience and default mode network coupling predicts cognition in aging and Parkinson's disease. J Int Neuropsychol Soc 22(2):205–215
Raichle ME (2015) The brain's default mode network. Annu Rev Neurosci 38:433–447
Raij TT, McEvoy L, Mäkelä JP et al (2000) Human auditory cortex is activated by omissions of auditory stimuli. Brain Res. 868(2):163–165
Recenti M, Ricciardi C, Aubonnet R et al (2021) Toward predicting motion sickness using virtual reality and a moving platform assessing brain, muscles, and heart signals. Front Bioeng Biotechnol 9:635661
Recenti M, Jacob D, Aubonnet R et al (2022) Predicting lifestyle using BioVRSea multi-biometric paradigms. 2022 IEEE International Conference on Metrology for Extended Reality. IEEE, Artificial Intelligence and Neural Engineering (MetroXRAINE), pp 329–334
Recenti M, Guerrini L, Lindemann A et al (2023) Heart rate variability during a complex postural control task with the BioVRSea paradigm. 2023 IEEE International Conference on Metrology for eXtended Reality. IEEE, Artificial Intelligence and Neural Engineering (MetroXRAINE), pp 876–881
Rubinov M, Sporns O (2010) Complex network measures of brain connectivity: uses and interpretations. Neuroimage 52(3):1059–1069
Sakkalis V (2011) Review of advanced techniques for the estimation of brain connectivity measured with EEG/MEG. Comput Biol Med 41(12):1110–1117
Schwarz ST, Afzal M, Morgan PS et al (2014) The 'swallow tail'appearance of the healthy nigrosome-a new accurate test of parkinson's disease: a case-control and retrospective cross-sectional mri study at 3t. PLoS One 9(4):e93814

Seitzman BA, Snyder AZ, Leuthardt EC et al (2019) The state of resting state networks. Top Magn Reson Imaging 28(4):189–196
Shirer W, Ryali S, Rykhlevskaia E et al (2012) Decoding subject-driven cognitive states with whole-brain connectivity patterns. Cereb Cortex 22(1):158–165
Shumway-Cook A, Woollacott MH (2007) Motor control: translating research into clinical practice. Lippincott Williams & Wilkins
Singh A (2023) Evoked midfrontal activity predicts cognitive dysfunction in parkinson's disease. Brain 146(2):552–56. https://doi.org/10.1093/brain/awac367
Sridharan D, Levitin D, Menon V (2008) A critical role for the right fronto-insular cortex in switching between central-executive and default-mode networks. Proc Natl Acad Sci 105(34):12569–12574
Stehle SA, Aubonnet R, Hassan M et al (2022) Predicting postural control adaptation measuring EEG, EMG, and center of pressure changes: BioVRSea paradigm. Front Hum Neurosci 16:1038976
Tessitore A, Giordano A, De Micco R et al (2014) Sensorimotor connectivity in parkinson's disease: the role of functional neuroimaging. Front Neurol 5:180
Tolosa E, Wenning G, Poewe W (2006) The diagnosis of parkinson's disease. Lancet Neurol 5(1):75–86
Vossel S, Geng JJ, Fink GR (2014) Dorsal and ventral attention systems: distinct neural circuits but collaborative roles. Neuroscientist 20(2):150–159
Winter DA (1995) Human balance and posture control during standing and walking. Gait Posture 3(4):193–214
Woo H, Lee K (2019) The influence of postural control training on alpha band power during balance tasks. J Neurophysiol 122(5):1934–1942
Woollacott M, Shumway-Cook A (2002) Attention and the control of posture and gait: a review of an emerging area of research. Gait Posture 16(1):1–14
Xia M, Wang J, He Y (2013) Brainnet viewer: a network visualization tool for human brain connectomics. PLoS One 8(7):e68910
Xu D, Cole MH, Mengersen K et al (2014) (2014) Executive function and postural instability in people with Parkinson's disease. Parkinson's disease 1:684758
Yao N, Pang S, Cheung C et al (2015) Resting activity in visual and corticostriatal pathways in Parkinson's disease with hallucinations. Parkinsonism Relat Disord 21(2):131–137
Zhang W, Han X, Qiu S et al (2022) Analysis of brain functional network based on EEG signals for early-stage Parkinson's disease detection. IEEE Access 10:21347–21358
Zhu Z, Wang H, Bi H et al (2023) Dynamic functional connectivity changes of resting-state brain network in attention-deficit/hyperactivity disorder. Behav Brain Res 437:114121